Published in final edited form as:
Biochemistry. 2013 July 9; 52(27): . doi:10.1021/bi400470s.

Remarkable Stabilization of Plasminogen Activator Inhibitor 1 in a "Molecular Sandwich" Complex

Galina Florova[‡], **Sophia Karandashova**[‡], **Paul J. Declerck**[†], **Steven Idell**[‡], and **Andrey A. Komissarov**[‡,*]

[‡]Texas Lung Injury Institute of the University of Texas Health Science Center at Tyler, 11937 US Highway 271, Tyler, TX 75708-3154, USA

[†]Laboratory for Pharmaceutical Biology, Faculty of Pharmaceutical Sciences, Katholieke Universiteit Leuven, Leuven, Belgium

Abstract

Plasminogen activator inhibitor 1 (PAI-1) levels are elevated in a number of life threatening conditions and often correlate with unfavorable outcomes. Spontaneous inactivation due to active to latent transition limits PAI-1 activity *in vivo*. While endogenous vitronectin (Vn) stabilizes PAI-1 by 1.5–2.0 fold, further stabilization occurs in a "Molecular Sandwich" Complex (MSC) where a ligand that restricts the exposed reactive center loop is bound to PAI-1/Vn. The effects of S195A two chain urokinase (tcuPA) and Vn on inactivation of wild type (wt) glycosylated (Gl-PAI-1), non-glycosylated (rPAI-1) and non- glycosylated Q123K PAI-1 (lacks Vn binding) were studied. S195A tcuPA decreased the rate constant (k_L) for spontaneous inactivation at 37°C for rPAI-1, Q123K, and Gl-PAI-1 by 6.7, 3.4, and 7.8 fold, respectively, and with both S195A tcuPA and Vn by 66.7, 5.5, and 103.3 fold. Analysis of the temperature dependences of k_L revealed a synergistic increase in the Gibbs free activation energy for spontaneous inactivation of wt Gl-PAI-1 and rPAI-1 in MSC from 99.8 and 96.1 to 111.3 and 107.0 kJ/mol, respectively, due to an increase in the activation enthalpy and a decrease in the activation entropy. Anti-PAI-1 mAbs competing with proteinase also stabilize PAI-1/Vn. The rate of inhibition of target proteinases by MSCs, with stoichiometry close to unity, was limited by the dissociation ($k=10^{-4}$–10^{-3} s^{-1}) of S195A tcuPA or mAb. The stabilization of PAI-1 in MSCs *in vivo* may potentiate uncontrolled thrombosis or extravascular fibrin deposition, suggesting a new paradigm for using PAI-1 inhibitors and novel potential targets for therapy.

Keywords

active PAI-1; vitronectin; S195A tcuPA; mAb; molecular sandwich; stabilization

Plasminogen activator inhibitor-1 (PAI-1) is a major endogenous inhibitor of tissue- (tPA) and urokinase-type (uPA) plasminogen activators, and contributes to the regulation of normal and pathological thrombolysis and fibrinolysis, cell migration, and participates in multiple signaling pathways (1–4). Since elevated plasma levels of PAI-1 antigen (5–8) and activity (8–10) correlate with severity and unfavorable outcomes in a number of diseases, PAI-1 is considered a biomarker and potential molecular target for therapeutics.

[*]Corresponding Author: The University of Texas Health Science Center at Tyler (UTHSCT), 11937 US Highway 271, Tyler, TX 75708, USA; phone: 903 877 5183 Fax: 903 877 5627; andrey.komissarov@uthct.edu.

DISCLOSURES

Authors disclose no conflict of interest.

Mechanism-based inhibition of proteinases by PAI-1 (Scheme 1) starts by binding the enzyme at the docking site, resulting in the formation of a Michaelis complex (MC). Next, the cleavage of the scissile bond of the reactive center loop (RCL) of PAI-1 and the formation of an acyl-enzyme triggers massive conformational changes, resulting in the rapid insertion of the RCL (k_{lim1}) as strand 3 into central β-sheet A, and the translocation of the bound enzyme to the opposite pole of PAI-1 (Scheme 1). Mechanical distortion of the native structure of the enzyme results in its stabilization, forming an inhibitory complex (SIC, Scheme 1). Proteinases differ in the rate of RCL insertion (k_{lim1}; Scheme 1), which limits the rate of inhibition of the enzyme by PAI-1. The stoichiometry of inhibition, the number of PAI-1 molecules required to inhibit one molecule of the enzyme (11), is close to unity for the reactions with tPA and uPA. Active PAI-1 is a kinetically trapped, metastable conformation of the serpin, which spontaneously converts to a thermodynamically stable, inactive, latent PAI-1 (Scheme 1). The slow transition of PAI-1 to its latent conformation due to the spontaneous insertion of uncleaved RCL to the β-sheet A (k_{L1}, Scheme 1) prevents accumulation of active PAI-1 and limits its endogenous activity. Under physiological conditions, the active conformation of PAI-1 has a short half-life ($t_{1/2}$), ranging between 1.5 and 2.0 h (12).

Vitronectin (Vn), a cell adhesive glycoprotein, approaches micromolar levels of concentration in the circulation, and binds active PAI-1 with nanomolar affinity ($k_{-2}/k_{+2}< 10^{-8}$ M; Scheme 1) (13–15). Vn stabilizes the active conformation of PAI-1, decreasing its rate of spontaneous inactivation (k_{L1}/k_{L2}=1.5–2.0; Scheme 1) (16;17). Vn dissociates from PAI-1 after the insertion of its RCL (Scheme 1, (18)). Binding Vn induces conformational changes in the proteinase docking site, which further facilitate interactions between the RCL and the active site of the target enzyme (19) due to an increase in the rigidity of the PAI-1 molecule (20). The mechanism of inhibition of the enzyme by PAI-1/Vn includes the formation of a transient ternary “Molecular Sandwich” type complex (MSC) (Scheme 1). Vn often affects both the kinetics and stoichiometry of inhibition (21–29) for the reactions of PAI-1 with different enzymes. Binding Vn decreases the rate of RCL insertion ($k_{lim1}>k_{lim2}$; Scheme 1) for tcuPA, trypsin, and tctPA at pH<7.0 (26;27), but does not affect the stoichiometry of inhibition (24;26). Such a decrease in the limiting rate of RCL insertion (Scheme 1) reflects the stabilization of the ternary MSC, which, due to the abundance of endogenous Vn, is a part of the PAI-1 mechanism *in vivo*. A further decrease in k_{lim2} (stabilization of MSC; Scheme 1) was observed for the reactions of PAI-1/Vn with activated protein C (25;28) and factor VIIa/tissue factor (29) (for both $k_{lim2} \ll k_{lim2}$ for target proteinases; Scheme 1). Thus, transient MSCs with different stability occur *in vivo* and could contribute to normal and pathological fibrinolysis and cell signaling.

Finally, inactive proteinases such as anhydrotrypsin (trypsin with dehydroalanine at the position 195; chymotrypsin numbering), and S195A mutant variants of tPA and uPA (30–33), when bound to PAI-1/Vn, form a stable MSC (k_{lim2}= 0; Scheme 1). While binding Vn ($k_{+2;}$ Scheme 1) and inactive proteinases (k_{+1}; Scheme 1) are among the mechanisms that stabilize active PAI-1 ($k_{L1}>k_{L2}$, and $k_{L1}> k_{L3}$; Scheme 1) (2;4), to the best of our knowledge, there is a lack of data on the stability of the active conformation of PAI-1 in stable (k_{lim2}= 0; Scheme 1) MSCs (k_{L4}, Scheme 1). A model of the MSC (Figure 1) based on known X-ray structures of active PAI-1 bound to S195A tcuPA (33) and somatomedin B (SMB) domain of Vn (34) shows ligands bound to opposite poles of the PAI-1 molecule. Here we demonstrate that S195A, tcuPA, and Vn synergistically stabilize the active conformation of PAI-1, increasing the $t_{1/2}$ for its spontaneous inactivation up to almost two orders of magnitude. Moreover, we demonstrate that anti-PAI-1 monoclonal antibodies (mAbs), which compete for PAI-1 with proteinase (35), also stabilize active PAI-1.

EXPERIMENTAL PROCEDURES

Proteins and Reagents

Monomeric Vn, wt non-glycosylated (r), glycosylated (Gl-) PAI-1, non- glycosylated Q123K PAI-1 (lacks vitronectin binding), and three mutant variants of PAI-1 with introduced cysteines labeled with N-((2-(iodoacetoxy) ethyl)-N-methyl) amino-7-nitrobenz-2-oxa-3-diazole (NBD) - S338C (NBD P9) PAI-1, M447C (NBD P1′) PAI-1 and S119C (NBD S119C) PAI-1 were purchased from Molecular Innovations (Novi, MI). E350A/E351A NBD P9 PAI-1 was obtained and characterized as previously described (36). S356A (S195A in chymotrypsin numbering) recombinant catalytically inactive scuPA was generated and purified, as previously described (37;38). The proenzyme was converted to the two-chain form by incubation with the resin with immobilized plasmin (Molecular Innovation, Novi MI) as previously described (39). Complete activation was confirmed with SDS PAGE under reducing conditions, as described in (40). Urokinase activity standard (100,000 IU/mg) was from American Diagnostica (Stanford, CT); recombinant tcuPA was a gift from Abbott Laboratories (Chicago, IL); recombinant single chain tPA (sctPA) (Activase) was from Genentech (San Francisco, CA). Glu-plasminogen (Plg), plasmin (PL), and fluorogenic PL substrate were from Haematologic Technologies Inc. (HTI, Essex Junction, VT). Fluorogenic tPA and uPA substrates were from Centerchem Inc. (Norwalk, CT). All experiments were carried out in 20 mM Hepes/NaOH buffer, pH 7.4, containing 0.13M NaCl.

Effects of S195A tcuPA and Anti-PAI-1 mAbs on the Spontaneous Inactivation of PAI-1 and PAI-1/Vn

Time-dependent spontaneous inactivation of rPAI-1, Q123K PAI-1, Gl-PAI-1 and their complexes with Vn, S195A tcuPA, anti-PAI-1 mAbs MA-56A7C10, MA-42A2F6, MA-44E4 and two ligands (MSC formed in the presence of Vn and either S195A tcuPA or mAb) was studied by incubating the serpins (0.25–2.5 μM), with one or two ligands taken at 1.0–2.0 molar excess in 20 mM Hepes/NaOH buffer, pH 7.4, containing 0.13 M NaCl, at 37°C for 0–720 h. The concentration of active PAI-1 was determined by two independent methods as previously described (9;41). First, active PAI-1 in aliquots withdrawn at 0–168 h was titrated with increasing amounts of sctPA or tcuPA with known specific activity, followed by measuring the residual tPA or uPA amidolytic activity. The concentration of active PAI-1 in aliquots was determined from the linear calibration plots obtained from titration of known amounts of active PAI-1 with the same standard solutions of sctPA or tcuPA (9;41). The same aliquots were incubated with 1.2–2.5 molar excess (over PAI-1) of sctPA for 30–60 min at 37°C followed with analysis of the reaction products by SDS PAGE (NuPAGE Novex 4–12% Bis-Tris Midi gels; Invitrogen, Grand Island, NY). Proteins were visualized by staining with SYPRO Ruby protein gel stain (Invitrogen, Grand Island, NY). To estimate active PAI-1, gels were scanned and analyzed using a Molecular Imager equipped with Quantity One (version 4.2.3) software (Bio-Rad Laboratories, Hercules, CA). The amounts of PAI-1 (latent, cleaved, and complexed with proteinase (SIC; Scheme 1) were estimated from the intensity of the corresponding bands and active PAI-1 (50% of density in SIC) was expressed as percent of total PAI-1 density. After one month (720 h) of incubation at 37°C, PAI-1 activity was determined by two independent methods with higher levels of sensitivity: (i) PAI-1 inhibition of tcuPA mediated Plg activation and (ii) visualization of the PAI-1 at the gel (PAI-1/tPA complex (SIC)), latent and cleaved PAI-1) by Western blotting using IBlot™ (Invitrogen, Grand Island, NY) as described elsewhere (9;41).

Measurement of tPA, uPA and PL Amidolytic Activity

Amidolytic activities of tPA and uPA were estimated from the time-increase in fluorescence emission at 440 nm (excitation 344 nm) of 0.2 mM fluorogenic substrates (Pefafluor tPA CH_3-SO_2-D-Phe-Gly-Arg-AMC AcOH and Pefafluor uPA Bz-β-Ala-Gly-Arg-AMC AcOH, respectively; where AMC is 7-amino-4-methylcoumarin; Centerchem Inc, (Norwalk, CT)). PL activity was measured using fluorogenic substrate (D-Ala-Phe-Lys-ANS-NH-iC_4H_9·2HBr; where ANS is 6-amino-1-naphthalenesulfonamide; HTI, Essex Junction, VT) and calculated from an increase in fluorescence emission at 470 nm (excitation at 352 nm) as previously described (9;38;41). Amidolytic activity was measured in either white or black 96-well flat bottom plates from Costar (Corning Inc, NY) using a Varian Cary Eclipse fluorescence spectrophotometer (Varian Inc, IL) or Synergy™ HT Hybrid Reader (BioTek, Winooski, VT), respectively.

Stoichiometry of Inhibition *for Inhibition of uPA and tPA by MSC*

The stoichiometry of inhibition is the number of moles of PAI-1 required for the inactivation of one mole of proteinase (11). The effects of binding of S195A tcuPA alone and with Vn on stoichiometry of inhibition for tPA and uPA were determined directly by titration of binary complexes (S195A tcuPA/PAI-1 variant) and MSCs (Scheme 3) with proteinase using Varian Cary Eclipse fluorescence spectrophotometer. Briefly, the known amount (20–100 nM) of binary or ternary complex was incubated with increasing amounts of the proteinase for 30 min at 37°C. A residual enzyme activity was determined using fluorogenic substrate as previously described (38;42). Starting from the equivalence point (complete neutralization of the PAI-1 variant), the addition of proteinase resulted in measurable (limit of detection 0.1 nM) enzymatic activity. The stoichiometry of inhibition for complexes with NBD P9 PAI-1 was determined as described previously (43). The values of the stoichiometry of inhibition (average of 2–3 experiments) were calculated as a ratio of moles of active PAI-1 in the complex and moles of the proteinase used to reach the equivalence point. The stoichiometry of inhibition for the reaction of 1.2–2.5 fold molar excess of tPA or uPA and rPAI-1, Gl-PAI-1, Q123K PAI-1 and their complexes with S195A tcuPA, Vn, or both ligands was also estimated from SDS PAGE analysis as described elsewhere (9;41;43).

Kinetics of Formation and Dissociation of MSC

NBD P1′, NBD S119C and NBD P9 mutant variants of PAI-1 were used to measure the second order association rate constants (k_{+1}, k_{+2}, k_{+3} and k_{+4} Scheme 1) for the formation of MSC and binary complexes using stopped flow fluorimetry as previously described (26;43;44). An NBD PAI-1 variant (or its complex with one ligand; 10–50 nM) was mixed with increasing concentrations of the ligand (second ligand) in a microvolume stopped-flow reaction analyzer (model SX-20, Applied Photophysics Ltd, Leatherhead, UK), equipped with a fluorescence detector and a thermostated (25°C) cell. The progress of the reaction was monitored as an increase in the NBD fluorescence emission via a 515 nm cutoff filter (excitation 490 nm). Pro-Data Viewer software (Applied Photophysics Ltd, Leatherhead, UK) was used to fit a single-exponential equation $F_t = F_\infty + A_1 * e^{-(kobs)t}$) to the data (where k_{obs} is the first order rate constant of the complex formation, F_t, F_∞ and A are fluorescence emission at time t, at infinite time, and the amplitude, respectively). Diffusion limited association rate constants (k_{+1}, k_{+2}, k_{+3} and k_{+4}, Scheme 1) were determined from the slopes of linear k_{obs} on ligand concentration using SigmaPlot 11.0 (SPSS Inc., San Jose, CA). Dissociation rate constants (k_{-1}, and k_{-4}, Scheme 1) for complexes of NBD P1′, NBD P9, and P4′P5′/AA NBD P9 PAI-1 variants with S195A tcuPA were determined in a manner similar to that described previously for the reaction between PAI-1 and prourokinase (38). Briefly, preformed complexes were rapidly mixed with an excess of tcuPA or sctPA in the SX-20 and the progress of the reaction was monitored via changes in the NBD fluorescence emission with time. The values of k_{obs} were calculated by fitting a single exponential

equation to the data and plotted against proteinase concentration. A linear equation $k_{-} = k_{obs}$ (where k_{-} are k_{-1} and k_{-4}) was fit to the data using SigmaPlot 11.0 (SPSS Inc., San Jose, CA). The values of k_{-1} and k_{-4} for unlabeled variants of PAI-1 (wt rPAI-1, Gl-PAI-1 and Q123K PAI-1) were determined using the competition of NBD P1′ PAI-1 with unlabeled variants for S195A tcuPA for S195A tcuPA. Briefly, preformed complexes of unlabeled PAI-1 variants (5–20 nM) with 1.0–1.2 molar excess of S195A tcuPA were mixed with NBD P1′ PAI-1 (40–250 nM) using the SX-20, k_{obs} were calculated from changes in the NBD fluorescence emission with time, plotted versus [NBD P1′ PAI-1], and a linear equation $k_{-} = k_{obs}$ (where k_{-} are k_{-1} and k_{-4}) was fit to the data using SigmaPlot 11.0 (SPSS Inc., San Jose, CA).

The affinities of PAI-1 and its variants (with or without Vn present) to S195A tcuPA were determined in a manner similar to that described for anti-PAI-1 mAbs (43). The affinity of S195A tcuPA to NBD P9 PAI-1 was estimated from the dependence of k_{obs} for the reaction of tctPbA with 0.5–5.0 nM NBD P9 PAI-1 (NBD P9 PAI-1/Vn) preincubated for 15 min with increasing amounts of S195A tcuPA. The affinity of wt r-, Gl-PAI-1, and Q123K PAI-1 was estimated from the dependences of the initial rates of amidolytic activity of tPA on the concentration of S195A tcuPA after mixing of 0.5–5 nM PAI-1 or its variants preincubated for 15 min with increasing amounts of S195A tcuPA (with or without Vn) with equimolar amount of tctPA and Pefafluor tPA (0.2 mM).

Interaction of NBD P1′ PAI-1 with tcuPA

The simplest mechanism of the reaction between serpin (I) and proteinase (E), (Scheme S1), includes the Michaelis complex (E·I), followed by the formation of a stable inhibitory complex (E-I*). A change in the fluorescence emission of the P1′ NBD group reports both the formation of the Michaelis complex (an increase in the NBD fluorescence emission; Figure S4; Inset) and the dissociation of the enzyme from the initial docking site due to RCL insertion (a decrease in the NBD fluorescence emission) (44). The two corresponding values of k_{obs} were calculated by fitting a double exponential equation ($F_t = F_\infty + A_1e^{-(kobs1)t} + A_2e^{-(kobs2)t}$) using Pro-Data Viewer software (Applied Photophysics Ltd, Leatherhead, UK) to the recorded changes in the P1′ NBD fluorescence.

k_{lim} and K_M were calculated by fitting the dependence of k_{obs1} on enzyme concentration with a hyperbolic equation $k_{obs1} = k_{lim}*[E]/(K_M + [E])$ (where k_{lim} is the first order rate constant at the infinite concentration of the enzyme, and $K_M = (k_{lim} + k_{-1})/k_1$ is the concentration of the enzyme at $k_{obs1} = k_{lim}/2$) as described previously (26;43). Values k_{+1} and k_{-1} (Scheme S1) were calculated by fitting a linear equation $k_{obs2} = k_{lim} + k_{-1}) + k_1$ [enzyme] to the linear dependence of the fast k_{obs2} on the enzyme concentration as described (44).

Effects of Temperature on the Rate of Spontaneous RCL Insertion Due to the Active to Latent Transition of PAI-1 Variants and Their Complexes with Vn and S195A tcuPA — The temperature dependences (37–60°C) of the k_{L1}, k_{L2}, k_{L3} and $k_{L4,}$ respectively (Scheme 1) for rPAI-1, Gl-PAI-1 and Q123K PAI-1, their complexes with Vn, S195A tcuPA and both ligands were analyzed as Eyring plots of $ln(k_L/T)$ or versus 1/T. The values of k_{L1}, k_{L2}, k_{L3} and $k_{L4,}$ respectively; (Scheme 1) for rPAI-1, Gl-PAI-1 and Q123K PAI-1 and their complexes with Vn, S195A tcuPA and both ligands were measured at 37, 50, 55 and 60°C. The activation enthalpy ($\Delta H^{‡}$) and entropy ($\Delta S^{‡}$) were determined from the Eyring plots of $ln(k_L/T)$ or versus 1/T, which linearly relates both parameters: $ln(k_L/T) = ln(k_B/h) + \Delta S^{‡}/R - \Delta H^{‡}/RT$, where T is the absolute temperature, and R, k_B, and h are 8.3145 J/mol, 1.3806×10^{-23} J/K and 6.626×10^{-34} J/s, respectively. The parameters of the best fit of the linear equation to the data (SigmaPlot 11.0, SPSS Inc., San Jose, CA) were used to calculate $\Delta H^{‡}$ and $\Delta S^{‡}$ as -(slope)×8.3145 J/mol and (intercept - 23.76)×8.3145 J/mol K, respectively.

The values of the Gibbs free activation energy ($\Delta G^{\ddagger}$) for the spontaneous active to latent transition of PAI-1 variants and their complexes were calculated as $\Delta G^{\ddagger} = \Delta H^{\ddagger} - T\Delta S^{\ddagger}$. To evaluate the dependence between contributions of $\Delta H^{\ddagger}$ and $\Delta S^{\ddagger}$ to $\Delta G^{\ddagger}$ for spontaneous inactivation of wt Gl-PAI-1, rPAI-1, Q123K PAI-1 alone or in the presence of Vn, S195A tcuPA or both ligands, the values of $\Delta H^{\ddagger}$ were plotted as a function of $-T\Delta S^{\ddagger}$. A linear equation was fit to the data using SigmaPlot 11.0. (SPSS Inc., San Jose, CA).

Additivity in the Effects of S195A tcuPA and Vn on the Active to Latent Transition of PAI-1

The additivity in the effects of Vn and S195A tcuPA on the spontaneous inactivation of PAI-1 variants was tested by comparing changes in the $\Delta G^{\ddagger}$ ($\Delta\Delta G^{\ddagger}$) caused by Vn, S195A tcuPA ($\Delta\Delta G^{\ddagger}_{Vn}$ and $\Delta\Delta G^{\ddagger}_{S195A\ tcuPA}$, respectively) and both ligands together ($\Delta\Delta G^{\ddagger}_{Vn/S195A\ tcuPAl}$), assuming additivity if $\Delta\Delta G^{\ddagger}_{Vn/S195A\ tcuPAl} = \Delta\Delta G^{\ddagger}_{Vn} + \Delta\Delta G^{\ddagger}_{S195A\ tcuPA}$ and if $\Delta\Delta G^{\ddagger}_{Vn/S195A\ tcuPAl} > \Delta\Delta G^{\ddagger}_{Vn} + \Delta\Delta G^{\ddagger}_{S195A\ tcuPA}$, the effect is synergistic. The values of $\Delta\Delta G^{\ddagger}$ were presented as a bar graph.

Effects of MSC on the Acceleration of Active to Latent Transformation by mAb MA-33B8

NBD P9 PAI-1 (10–20 nM) and its complexes with Vn (20–50 nM), MSC with S195A tcuPA (20–50 nM), or 20–50 nM of mAbs MA-56A7C10, MA-42A2F6 or MA-44E4, were incubated with MA-33B8 (50–400 nN) in 96-well flat bottom plates from Costar (Corning Inc, NY) and increases in NBD fluorescence with time were measured using a fluorescence spectrophotometer Synergy™ HT Hybrid Reader (BioTek, Winooski, VT). The k_{obs} were calculated by fitting a single exponential equation to the data using Gen5™ 2.0 Data Analysis Software (BioTek, Winooski, VT) and SigmaPlot 11.0 (SPSS Inc., San Jose, CA), as described elsewhere (26;43;45) and plotted against the concentration of MA-33B8 (46).

Data Analysis

Pro-Data Viewer software (Applied Photophysics Ltd, Leatherhead, UK) was used to analyze stopped-flow fluorescence traces. All of the measurements were carried out under pseudo-first-order kinetics conditions (the concentration of the ligand or proteinase was at least five-fold higher than that of a PAI-1 variant or its complexes). The values of the correlation coefficient (r^2>0.90 for all of the kinetic data) and visual analysis of the plots of the residuals (deviation of the fitted function from the actual data) were used to estimate the quality of the fit. The values of k_{obs} (average of 4–6 measurements; S.E. less than 10%) were plotted against the molar concentration of proteinase or ligand.

RESULTS AND DISCUSSION

Formation and Dissociation of the MSC and its Interaction with Target Proteinases. (Scheme 1)

Three mutant variants of PAI-1: wild type recombinant non-glycosylated (rPAI-1), glycosylated (Gl-PAI-1), which was recently shown to be more stable than rPAI-1 (47), and a non-glycosilated mutant variant that lacks Vn binding ability (Q123K PAI-1) (48) were selected to compare the contribution of glycosylation and Vn binding to the stabilization of the active conformation of PAI-1 in MSCs. The kinetics of MSC formation between PAI-1, Vn, and S195A tcuPA (Figure 1; Scheme 1) and its interaction with tcuPA and tPA were studied in order to determine the association and dissociation rate constants (Scheme 1) and evaluate the effect of the ligands on the stoichiometry of inhibition for the reactions with target proteinases. A number of rPAI-1 mutant variants with a NBD-group attached to a single cysteine at positions P9 (reports RCL insertion (49)), P1′ (reports MC formation and movement of primed part of cleaved RCL (44)) and 119 (reports binding of Vn) were used to evaluate the kinetics of PAI-1 interaction with S195A tcuPA and Vn (Scheme 1). The values of k_{+1}, k_{+2}, k_{+3}, k_{+4} (Scheme 1) were determined using stopped flow fluorimetry as

previously described (26;43–45) from the slopes of linear dependences of k_{obs} on the concentration of ligand (Figure 2; Table 1). Diffusion limited k_{+1} and k_{+4} (4.0–8.0 $\mu M^{-1}s^{-1}$; Figure 2; Table 1) were determined measuring the time traces of changes in fluorescence emission (excitation 490 nm) of NBD P9, NBD P1′, and NBD S119C PAI-1 (k_{+1}) or their complexes with Vn (k_{+4}), due to the interaction with S195A tcuPA. Values of k_{+2} and k_{+3} (7.5 and 13.3 $\mu M^{-1}s^{-1}$, respectively; Figure 2; Table 1) were determined in a similar manner using NBD S119C PAI-1 (free or complexed with S195A tcuPA, respectively) and Vn. The second order rate constants for interaction of S195A tcuPA with PAI-1 or PAI-1/Vn (k_{+1} and k_{+4}, respectively; Table 1) were almost an order of magnitude lower than the association rate constant (k_{on}=27 ± 1 $\mu M^{-1}s^{-1}$) for the interaction between S195A tPA and NBD P9 PAI-1 (32). However, when the contribution of ionic exosite interactions is minimized (0.5 M Hepes) the value of k_{on} (4.5 ± 0.1 $\mu M^{-1}s^{-1}$ (32)) becomes comparable to those for S195A tcuPA (Table 1). These results support the hypothesis of weaker exosite interactions between PAI-1 and uPA when compared to tPA (50) and demonstrate that binding Vn does not significantly change the second order rate constant for interaction between PAI-1 and S195A tcuPA.

S195A tcuPA when bound to PAI-1 in a binary complex or in MSC (Figure 1) occupies the proteinase docking site (Scheme 1). Thus, neither of the two complexes is able to interact directly with the target proteinases. As a result, the dissociation of S195A tcuPA from PAI-1 or PAI-1/Vn (k_{-1} and k_{-4}, respectively, Scheme 1) limits the rate of the reaction with tcuPA or tPA. NBD P9 PAI-1, which reports the insertion of the RCL into central β-sheet A due to the reaction with proteinase (Scheme 1) by a 6 fold increase in the fluorescence emission of the NBD-group (49) and is biochemically similar to the wtPAI-1 (36;44;49;51;52), was used to determine rates of dissociation of S195A tcuPA. As expected (Figure 2), the observed rate constants (k_{obs}) for the reaction of the S195A tcuPA/NBD P9 PAI-1 or the corresponding MSC with tcuPA or tPA were independent of enzyme concentration (k_{-1}= (6.0 ± 0.3) $\times 10^{-3}$ and k_{-4}=(4.0 ± 0.2) $\times 10^{-3}$ s^{-1}, Table 1; Scheme 1; Figure 2). The values of k_{obs} for the inhibition of tPA and tcuPA with complexes of S195A tcuPA and rPAI-1, Gl-PAI-1, or Q123K PAI-1 (with or without Vn), which were measured in the presence of fluorogenic substrate (29), were also low ((3.0–7.0) $\times 10^{-3}$ s^{-1}; Table 1) and independent of the enzyme concentration. Similar values of K_D, k_{-1}, and k_{-4} (Table 1) observed for different mutant variants of PAI-1 (with an exception of NBD P1′ PAI-1) indicate similar mechanisms driving the formation of MSCs. Therefore, high affinity binding of S195A tcuPA and Vn to PAI-1, which is determined by the diffusion limited (>1 μM^{-1} s^{-1}) association rate constants, and slow (<10^{-2} s^{-1}) dissociation rate constants (Figure 2; Table 1), governs the stabilization of the MSC. Binding Vn, S195A tcuPA, or both ligands did not significantly affect the stoichiometry of inhibition for the reactions of every PAI-1 variant studied with either tPA or tcuPA (data not shown). Thus, active PAI-1 in a MSC (Figure 1) retains 100% capacity to inhibit equimolar amounts of target proteinase. However, in contrast to reactions of PAI-1 or PAI-1/Vn with target proteinases (Scheme 1), the rate of the reaction is limited by slow dissociation of S195A tcuPA.

The positively charged 37-loop of uPA or tPA could form exosite interactions with E350E351 (P4′P5′ nomenclature of Schechter and Berger (53)) of the RCL in PAI-1 (36;54;55) and thus, stabilize MSC. To determine the contribution of P4′P5′ (Figure 1) to the stabilization of MSCs, k_{-1} and k_{-4} (Scheme 1) for complexes of S195A tcuPA with P4′P5′/AA NBD P9 PAI-1 were determined. The values of k_{-1} and k_{-4} (7.0 ± 0.2 and 4.0 ± 0.2 × 10^{-3} s^{-1}, respectively; (Table 1)), were similar to those observed for the wt NBD P9 PAI-1 (Table 1). Therefore, the contribution of E350 and E351 to dissociation of the MSC or binary complex (k_{-4} and k_{-1}, respectively, Scheme 1) is rather insignificant. This conclusion supports the molecular model of S195A tcuPA/PAI-1 (Figure 1) which predicts that no direct interactions between 37-loop of uPA and P4′P5′ occur (Figure 1) (33). In

contrast to P4′P5′, the P1′ residue of the RCL contributes to the stabilization of a MSC. The introduction of an NBD labeled cysteine at the P1′ position (NBD P1′ PAI-1) resulted in an increase in both k_{-1} and k_{-4} by 22.5 and 25 fold, respectively, without significant changes in k_{+1} and k_{+4} when compared to NBD P9 PAI-1 (Table 1). To test whether or not exosite interactions other than P4′P5′ participate in the interaction between S195A tcuPA and PAI-1, the kinetics of the reaction between NBD P1′ PAI-1 and tcuPA were studied using stopped flow fluorimetry (Figure 3) and compared to that for NBD P9 PAI-1 (26;43;44). Similar to the reaction between NBD P1′ PAI-1 and tPA (44), biphasic changes in the NBD fluorescence emission were observed for the reaction between NBD P1′ PAI-1 and tcuPA (Figure 3; Inset) reflect the fast formation of a non-covalent transient intermediate complex between PAI-1 and the enzyme followed by dissociation of primed end of the cleaved RCL. In contrast to trypsin and similar to tPA (44), an increase in the K_D for NBD P1′ PAI-1, when compared to NBD P9 PAI-1 (Table 1), paralleled with an increase in corresponding K_M (Scheme 2) from 2.8 ± 0.6 to 10.0 ± 4.0 μM (Figure 3). Therefore, while P4′P5′ do not stabilize the MSC, other exosite interactions, which are perturbed by a mutation at the P1′, likely contribute to the binding of tcuPA to PAI-1 and to the stabilization of the MSC (Figure 1).

A MSC Slows Down the Spontaneous Inactivation of PAI-1 by Two Orders of Magnitude

Under conditions of k_{lim}=0 (Scheme 1), which are characteristic for both MC and MSC (Scheme 1) formed with S195A tcuPA, the spontaneous insertion of uncleaved RCL to β-sheet A due to the active to latent transition (k_{L1}, k_{L2}, k_{L3} and k_{L4}, Scheme 1) becomes the major mechanism of inactivation of PAI-1. Individually, Vn and S195A tcuPA stabilize the active conformation of PAI-1 (2;56). Based on the additivity of effects of mAbs and Vn on PAI-1 mechanism observed previously (26;43;57), we hypothesized that both ligands (Figure 1) affect stability of active PAI-1 conformation additively or even synergistically. To compare the effects of S195A tcuPA, Vn, and both ligands on the rate of spontaneous active to latent transition of PAI-1 (Scheme 1) under physiological conditions, wt rPAI-1 and Gl-PAI-1 were incubated either with each or both ligands in 0.02 M Hepes, 0.13 M NaCl, pH 7.4 at 37°C. In the control experiments, Gl-PAI-1 and rPAI-1 were incubated without ligands under the same conditions. Q123K PAI-1 (lacks ability to bind Vn (48)) was used to evaluate the contribution of possible non-specific interactions with Vn. Aliquots were withdrawn at 0, 1, 15, 90, and 720 h and incubated with excess sctPA for 0.5–1.0 h at 37°C followed by SDS PAGE analysis (Figure 4A). Active PAI-1 was visualized as SIC with tPA either by staining with SYPRO Ruby protein stain (0–90 h), or by Western blot analysis for PAI-1 antigen (720 h).

While at time points 0 and 1 h (Figure 4A) active PAI-1 was observed in every reaction mixture, only two (rPAI-1 and Gl-PAI-1 incubated with both Vn and S195A tcuPA) contained active serpin at 90 and 720 h (Figure 4A). Notably, active conformations of rPAI-1 and Gl-PAI-1 were detected by two independent methods: Western blotting (Figure 4A, lower panel), and inhibition of activation of human Glu-plasminogen (Plg) by tcuPA (Figure 4B) after 1 month (720 h) at 37°C. Therefore, S195A tcuPA and Vn slow down spontaneous PAI-1 inactivation at 37°C by almost two orders of magnitude and do not significantly affect the stoichiometry of inhibition for tPA (Figure 4A) or uPA (Figure 4). Since the stoichiometry of inhibition for the reaction between MSCs and target proteinases remains close to unity, PAI-1 in MSCs retains the ability to inactivate almost equimolar amounts of tPA or uPA significantly longer than free serpin or its complex with Vn (Scheme 1). While normal levels of endogenous PAI-1 in plasma are relatively low (6–80 ng/ml (58;59)), its concentration is elevated by up to three orders of magnitude in a number of pathological conditions (60;61). Thus, accumulation of endogenous active PAI-1 in MSCs could result in the inefficiency of S195A proteinase variants (and similar inhibitors, which

compete with target proteinases for active PAI-1) for neutralizing PAI-1 *in vivo.* Formation of MSCs protects endogenous PAI-1/Vn (low k_{L4}/k_{L2}, Figure 4; Scheme 1) from inactivation by preventing the spontaneous transition from active to latent form. Thus, accumulation of PAI-1, stabilized in the active conformation by MSCs, could result in an increased capacity to inactivate higher levels of target proteinases.

The Thermodynamics of Stabilization of PAI-1 in a MSC

To evaluate the forces governing the stabilization of the active conformation of PAI-1, rates of spontaneous inactivation of free rPAI-1, Gl-PAI-1, and Q123K PAI-1 and their complexes with one or both ligands were determined at 37, 50, 55, and 60°C for free serpins. PAI-1 activity was determined in the aliquots withdrawn at different time points by titrating with sctPA as previously described (9). The first order rate constants (k_{L1}, k_{L2}, k_{L3} and k_{L4}, Scheme 1) for rPAI-1, Gl-PAI-1, and Q123K PAI-1 in the presence of S195A tcuPA, Vn, and both ligands were estimated from the slopes of linear dependences of semilogarithmic plots of residual PAI-1 activity versus time (Figure 5). The values of k_{L1}, k_{L2}, k_{L3}, and k_{L4} were determined by titrating the residual active PAI-1 (Figure 5; filled symbols) present in aliquots withdrawn at different time points, with increasing amounts of sctPA. Rate constants at 50°C (Figure 5; empty symbols) and at 37°C (not shown) were also estimated from the results of SDS PAGE. The $k_{L1}^{\text{SDS PAGE}}$, $k_{L2}^{\text{SDS PAGE}}$, $k_{L3}^{\text{SDS PAGE}}$ and $k_{L4}^{\text{SDS PAGE}}$ were assessed from changes in PAI-1 activity with time, determined by densitometry of digitized images of SDS PAGE (Figure 5, empty symbols). Active PAI-1, which formed SIC, was estimated as a fraction of total PAI-1 (latent, cleaved and complexed with sctPA). While the measurements of amidolytic tPA activity are more accurate, only SDS PAGE analysis provides direct proof (formed SIC) of active PAI-1 in the aliquot. Both sets of rate constants (Figure 5; Inset) correlated with each other for all three PAI-1 variants studied. A decrease in k_L (k_{L1}/k_{L4}) at 50°C due to MSC formation approaches two orders of magnitude for Gl-PAI-1 and rPAI-1 (Figure 5, Inset). The values of k_{L1}, k_{L2}, k_{L3}, and k_{L4} for the temperatures studied are shown in Table 2.

To determine effects of Vn, S195A tcuPA, and both ligands on changes in the activation enthalpy ($\Delta H^{\ddagger}$), entropy ($\Delta S^{\ddagger}$), and Gibbs free energy ($\Delta G^{\ddagger}$) for the reaction of spontaneous inactivation of rPAI-1, Gl-PAI-1, and Q123K PAI-1 Eyring plots (Figure 6) were analyzed. The values of $\Delta H^{\ddagger}$ and $\Delta S^{\ddagger}$ (Table 3) were determined from linear Eyring plots (Figure 6). The enthalpy/entropy compensation plot (Figure 7) illustrates the difference in the effects of Vn, S195A tcuPA, and both ligands together on the contribution of the $\Delta H^{\ddagger}$ and $-T\Delta S^{\ddagger}$ to the $\Delta G^{\ddagger}$ at 37°C. Positive $\Delta H^{\ddagger}$ controls the stability of active PAI-1 and, due to a positive $\Delta S^{\ddagger}$, increasing the temperature results in an increase in the rate of spontaneous active to latent transition (Table 3). Vn induces a decrease in $\Delta S^{\ddagger}$, which governs the stabilization of both rPAI-1 and Gl-PAI-1 (Figure 7; Table 3). Stabilization of rPAI-1 and Q123K PAI-1 by S195A tcuPA (with or without Vn) is driven by a decrease in $\Delta S^{\ddagger}$. In contrast, Gl-PAI-1 is stabilized due to a significant increase in $\Delta H^{\ddagger}$ (Figure 7; Table 3). Such an increase in $\Delta H^{\ddagger}$ could indicate the formation of additional exosite interactions between S195A tcuPA and Gl-PAI-1 that further stabilize the exposed RCL.

The simplest mechanism of the transition from active (I_A) to latent (I_L) conformation of PAI-1 (Figure 8; Scheme 3) includes a transient intermediate ($I^{\ddagger}$), which exists in equilibrium with active PAI-1 (46). While moving the equilibrium towards the formation of $I^{\ddagger}$ results in an increase in the rate of spontaneous inactivation of PAI-1 (46), a decrease in the level of $I^{\ddagger}$ should suppress active to latent transition. Comparing the changes in the Gibbs free energy of activation ($\Delta\Delta G^{\ddagger} = \Delta G^{\ddagger}_0 - \Delta G^{\ddagger}_1$, where $\Delta G^{\ddagger}_0$ and $\Delta G^{\ddagger}_1$ correspond to free PAI-1 and its complex with the ligand(s), respectively; Figure 8; Scheme 3) allows to determine the contribution of Vn, S195A tcuPA, and both ligands together to the

stabilization of active conformation of PAI-1 variants. An increase in the $\Delta\Delta G^{\ddagger}$ (Scheme 3) in the presence of both Vn and S195A tcuPA equal or higher than the sum of the effects of each ligand indicates additive or synergistic stabilization of I_A, respectively. Values of $\Delta\Delta G^{\ddagger}$ induced by Vn ($\Delta\Delta G^{\ddagger}_{Vn}$), S195A tcuPA ($\Delta\Delta G^{\ddagger}_{S195A\ tcuPA}$), and both ligands ($\Delta\Delta G^{\ddagger}_{Vn/S195A\ tcuPA}$) at 37°C are shown in Figure 8 for the three variants of PAI-1 studied. Notably, $\Delta\Delta G^{\ddagger}_{Vn/S195A\ tcuPA}$ were similar for both wild type variants - rPAI-1 and Gl-PAI-1 (Figure 8). Moreover, since the increase in $\Delta G^{\ddagger}$ due to the binding of both ligands ($\Delta\Delta G^{\ddagger}_{Vn/S195A\ tcuPA}$) was higher (by 4.4 and 2.6 kJ/mol, for Gl-PAI-1 and rPAI-1, respectively) than $\Delta\Delta G^{\ddagger}_{Vn}+\Delta\Delta G^{\ddagger}_{S195A\ tcuPA}$ (Figure 8; Table 3) Vn and S195A tcuPA act synergistically. Under experimental conditions used in this study, Vn did not stabilize Q123K PAI-1 and its $\Delta\Delta G^{\ddagger}_{Vn/S195A\ tcuPA}$ was significantly lower than that for wt PAI-1 (Figure 8). However, some increase in $\Delta\Delta G^{\ddagger}_{Vn/S195A\ tcuPA}$ over $\Delta\Delta G^{\ddagger}_{S195A\ tcuPA}$ observed for Q123K PAI-1 (Figure 8; Table 3), could reflect the effects of non-specific binding of Vn. The synergistic effect of S195A tcuPA and Vn on the stability of PAI-1 ($\Delta\Delta G^{\ddagger}_{Vn/S195A\ tcuPA} > \Delta\Delta G^{\ddagger}_{Vn} + \Delta\Delta G^{\ddagger}_{S195A\ tcuPA}$; Figure 8) could originate from enhanced stabilization of the exposed RCL by S195A tcuPA bound to a less flexible PAI-1 molecule (20), and reflect a shift of the position of equilibrium (Figure 8, Scheme 3, (46)) from a transient pre-latent intermediate $I^{\ddagger}$ towards I_A (Scheme 3). A disruption of the binding of either of the two ligands results in a dramatic decrease in the stability of the active conformation of PAI-1 as it was observed with Q123K PAI-1 or both binary complexes (Figure 4, 5).

Notably, the values of $\Delta G^{\ddagger}$ observed for wt rPAI-1 were always lower than those found for wt Gl-PAI-1 (Table 3). Higher $\Delta G^{\ddagger}$ reflects the higher stability of the glycosylated serpin (alone and in complexes with the ligands), and supports a recent report (47). The difference in the stability between wt rPAI-1 and Gl-PAI-1 ($\Delta\Delta G^{\ddagger}_{Gl} = \Delta G^{\ddagger}_{Gl\text{-}PAI\text{-}1} - \Delta G^{\ddagger}_{rPAI\text{-}1}$) was 3.7, 2.9, 3.3, and 4.3 kJ/mol for free serpins and their complexes with Vn, S195A tcuPA and both ligands, respectively (Table 3). Thus, $\Delta\Delta G^{\ddagger}_{Gl}$ likely reflects the contribution of glycosylation of the PAI-1 molecule to the stabilization of active PAI-1 and its complexes.

Anti-PAI-1 mAbs form MSCs, Stabilize PAI-1/Vn, and Protect PAI-1 from Inactivation with MA-33B8

Anti-human PAI-1 mAb MA-33B8 significantly accelerates the spontaneous active to latent transition of PAI-1 and PAI-1/Vn (increases k_{L1} and k_{L2}; Scheme 1) by binding with high affinity to both pre-latent intermediate and latent PAI-1 ($I^{\ddagger}$ and I_L, respectively, Scheme 3) (46). To test whether active PAI-1 in MSCs is protected from inactivation, NBD P9 PAI-1, its complex with Vn, and its complex with both ligands (Vn and S195A tcuPA) was incubated with different amounts of MA-33B8 and the rate of active to latent transition was determined as previously described (46). The k_{obs} of RCL insertion was increased linearly with [MA-33B8] for NBD P9 PAI-1 and its complex with Vn, (Figure 9, (46)). In contrast, k_{obs} for MSCs was much lower and independent of concentration of MA-33B8 (Figure 9). Since the epitope of MA-33B8 does not overlap with the proteinase docking site (62), formation of a MSC likely restricts the movements of the RCL in the active PAI-1, and thus decreases the concentration of $I^{\ddagger}$ by shifting equilibrium (Scheme 3) towards the active conformation of PAI-1 (I_A).

To determine whether ligands other than proteinase could form MSCs with PAI-1/Vn and affect the rate of its spontaneous inactivation, anti-PAI-1 mAbs (MA-56A7C10, MA-42A2F6, and MA-44E4) that compete with proteinase (35) were tested. These mAbs interact with the PAI-1 with nanomolar affinity at epitopes close to the proteinase docking site (35), and form a MSC with PAI-1/Vn (k_{lim2}=0; Scheme 1), substituting for S195A tcuPA (Figure 1). Similar to S195A tcuPA, MA-56A7C10, MA-44E4 (Figure 9), and MA-42A2F6 (not shown) effectively protected NBD P9 PAI-1/Vn from inactivation with MA-33B8. Therefore, it is likely that anti-PAI-1 mAbs that compete for PAI-1 with target

proteinases, and S195A tcuPA affect reaction between PAI-1/Vn and MA-33B8 via the same mechanism.

To compare the effects of MSCs formed with S195A tcuPA and anti-PAI-1 mAbs on the rate of active to latent transition, MA-56A7C10, MA-42A2F6 (Figure 9; Inset), and MA-44E4 (not shown) were incubated with PAI-1/Vn at 37°C for 168 h and analyzed for the presence of PAI-1 in the active conformation, using SDS PAGE (Figure 9; Inset). Similar to S195A tcuPA, all three anti-PAI-1 mAbs, had k_{-1} and k_{-4} in the range of 10^{-4}–10^{-3} s^{-1} (not shown), formed MSCs and stabilized active PAI-1 (Figure 9; Inset). These results demonstrate that MSCs, which stabilize active PAI-1 by moving the equilibrium towards I_A (Figure 8, Scheme 3), are resistant to MA-33B8-type PAI-1 inhibitors.

Stabilization of endogenous PAI-1/Vn in MSCs is a novel mechanism that can generate durable antiproteinase activity. If operative *in vivo*, these complexes have a potential to create and promote fibrin deposition and profibrotic repair. Due to a stoichiometry of inhibition close to unity, MSCs are able to inactivate close to equimolar amounts of target proteinases. Active PAI-1 is a molecular target in fibrinolytic therapy (9;63) and cancer (64) and its neutralization improves outcomes in animal models (9;65;66). Thus, the possibility of MSCs formation *in vivo* should be considered if S195A inactive proteinases or mAbs competing for PAI-1 are used. The effects of MSCs on PAI-1 specificity and signaling cascades, as well as MSCs metabolism and mechanisms of clearance, have yet to be investigated. In addition, the relative effects of increasing the thermodynamic stability of PAI-1 (to a half-life of days) versus its normal clearance rate (a half-life of about 30 min) will need to be evaluated as an important factor that could affect PAI-1 activity. Nevertheless, redirection of the PAI-1 mechanism towards the substrate pathway by mAbs (26;28;43) or by low molecular weight inhibitors (66), could be used to neutralize MSCs.

While, to the best of our knowledge, there are no reports of endogenous MSCs, a significant increase in the level of active PAI-1 was reported in a number of severe pathologies (67;68). An increase of more than two orders of magnitude in the concentration of PAI-1 in sepsis, complicated parapneumonics, and empyema is accompanied by an increase in both PAI-1 activity and the fraction of the active PAI-1 present in the circulation or pleural fluids (67;68). Moreover, 1.5–2.5 fold increase in PAI-1 activity without changes in the total antigen was observed between days 1 and 3 in severe pediatric sepsis (68). While such an accumulation of the active PAI-1 could indicate its stabilization or/and slower clearance, this increase in PAI-1 activity has been strongly correlated with unresolved multiple organ failure and a lethal outcome (68). Recently, the mechanisms of PAI-1 overexpression were studied in an animal model of microbial sepsis that recapitulates human disease (69) and thus could provide further evaluation of PAI-1 as a prognostic factor (70–74) and possible target in severe sepsis and disseminated intravascular coagulation.

Acknowledgments

This work was supported by NHLBI grant P50 HL107186-02 and the Texas Lung Injury Institute, UTHSCT. We thank Genentech for providing sctPA.

ABBREVIATIONS

Gl-	glycosylated
mAb	monoclonal antibody
MC	Michaelis complex

MSC	"Molecular Sandwich" complex
NBD	N-((2-(iodoacetoxy)ethyl)-N-methyl)amino-7-nitrobenz-2-oxa-3-diazole
NBD P1′ PAI-1	Met447Cys PAI-1 with NBD-group attached to the cysteine
NBD P9 PAI-1	Ser338Cys PAI-1 with NBD-group attached to the cysteine
NBD S119C PAI-1	Ser119Cys PAI-1 with NBD-group attached to the cysteine
Q123K PAI-1	non- glycosylated Gln123Lys vitronecting reduced binding PAI-1 mutant
P4′P5′/AA NBD P9 PAI-1	a double mutant variant E350A/E351A of NBD P9 PAI-1
PAI-1	plasminogen activator inhibitor-1
Plg	human Glu-plasminogen
r	non-glycosylated
RCL	reactive center loop
S195A tcuPA	tcuPA with Ser195Ala substitution (chymotrypsin numbering)
sc	single chain
SIC	stable inhibitory complex
SMB	somatomedin B domain of vitronectin
$t_{1/2}$	half-life
tc	two chain
tPA	tissue type plasminogen activator
uPA	urokinase
Vn	vitronectin
wt	wild type

References

1. Iwaki T, Urano T, Umemura K. PAI-1, progress in understanding the clinical problem and its aetiology. Br J Haematol. 2012; 157:291–298. [PubMed: 22360729]
2. Van De Craen B, Declerck PJ, Gils A. The Biochemistry, Physiology and Pathological roles of PAI-1 and the requirements for PAI-1 inhibition in vivo. Thromb Res. 2012; 130:576–585. [PubMed: 22801256]
3. Czekay RP, Wilkins-Port CE, Higgins SP, Freytag J, Overstreet JM, Klein RM, Higgins CE, Samarakoon R, Higgins PJ. PAI-1: An Integrator of Cell Signaling and Migration. Int J Cell Biol. 2011; 2011:562481. [PubMed: 21837240]
4. Declerck PJ, Gils A. Three Decades of Research on Plasminogen Activator Inhibitor-1: A Multifaceted Serpin. Semin Thromb Hemost. 2013
5. Gando S, Nakanishi Y, Tedo I. Cytokines and plasminogen activator inhibitor-1 in posttrauma disseminated intravascular coagulation: relationship to multiple organ dysfunction syndrome. Crit Care Med. 1995; 23:1835–1842. [PubMed: 7587259]
6. Iba T, Kidokoro A, Fukunaga M, Sugiyama K, Sawada T, Kato H. Association between the severity of sepsis and the changes in hemostatic molecular markers and vascular endothelial damage markers. Shock. 2005; 23:25–29. [PubMed: 15614127]

7. Idell S, Girard W, Koenig KB, McLarty J, Fair DS. Abnormalities of pathways of fibrin turnover in the human pleural space. Am Rev Respir Dis. 1991; 144:187–194. [PubMed: 2064128]
8. Semeraro N, Ammollo CT, Semeraro F, Colucci M. Sepsis, thrombosis and organ dysfunction. Thromb Res. 2012; 129:290–295. [PubMed: 22061311]
9. Karandashova S, Florova G, Azghani AO, Komissarov AA, Koenig K, Tucker TA, Allen TC, Stewart K, Tvinnereim A, Idell S. Intrapleural adenoviral delivery of human plasminogen activator inhibitor-1 exacerbates tetracycline-induced pleural injury in rabbits. Am J Respir Cell Mol Biol. 2013; 48:44–52. [PubMed: 23002099]
10. Balsara RD, Xu Z, Ploplis VA. Targeting plasminogen activator inhibitor-1: role in cell signaling and the biology of domain-specific knock-in mice. Curr Drug Targets. 2007; 8:982–995. [PubMed: 17896950]
11. Chaillan-Huntington CE, Gettins PGW, Huntington JA, Patston PA. The P6-P2 region of serpins is critical for proteinase inhibition and complex stability. Biochemistry. 1997; 36:9562–9570. [PubMed: 9236002]
12. Kruithof EK. Plasminogen activator inhibitors--a review. Enzyme. 1988; 40:113–121. [PubMed: 3139400]
13. Wiman B, Almquist A, Sigurdardottir O, Lindahl T. Plasminogen activator inhibitor 1 (PAI) is bound to vitronectin in plasma. FEBS Lett. 1988; 242:125–128. [PubMed: 2462509]
14. Tomasini BR, Mosher DF. Vitronectin. Prog Hemost Thromb. 1991; 10:269–305. [PubMed: 1706881]
15. Preissner KT, Seiffert D. Role of vitronectin and its receptors in haemostasis and vascular remodeling. Thromb Res. 1998; 89:1–21. [PubMed: 9610756]
16. Declerck PJ, De Mol M, Alessi MC, Baudner S, Paques EP, Preissner KT, Muller-Berghaus G, Collen D. Purification and characterization of a plasminogen activator inhibitor 1 binding protein from human plasma. Identification as a multimeric form of S protein (vitronectin). J Biol Chem. 1988; 263:15454–15461. [PubMed: 2459123]
17. Preissner KT, Grulich-Henn J, Ehrlich HJ, Declerck P, Justus C, Collen D, Pannekoek H, Muller-Berghaus G. Structural requirements for the extracellular interaction of plasminogen activator inhibitor 1 with endothelial cell matrix- associated vitronectin. J Biol Chem. 1990; 265:18490–18498. [PubMed: 1698787]
18. van Meijer M, Gebbink RK, Preissner KT, Pannekoek H. Determination of the vitronectin binding site on plasminogen activator inhibitor 1 (PAI-1). FEBS Lett. 1994; 352:342–346. [PubMed: 7523190]
19. Fa M, Karolin J, Aleshkov S, Strandberg L, Johansson LB, Ny T. Time-resolved polarized fluorescence spectroscopy studies of plasminogen activator inhibitor type 1: conformational changes of the reactive center upon interactions with target proteases, vitronectin and heparin. Biochemistry. 1995; 34:13833–13840. [PubMed: 7577977]
20. Trelle MB, Hirschberg D, Jansson A, Ploug M, Roepstorff P, Andreasen PA, Jorgensen TJ. Hydrogen/Deuterium Exchange Mass Spectrometry Reveals Specific Changes in the Local Flexibility of Plasminogen Activator Inhibitor 1 upon Binding to the Somatomedin B Domain of Vitronectin. Biochemistry. 2012
21. Ehrlich HJ, Gebbink RK, Keijer J, Linders M, Preissner KT, Pannekoek H. Alteration of serpin specificity by a protein cofactor. Vitronectin endows plasminogen activator inhibitor 1 with thrombin inhibitory properties. J Biol Chem. 1990; 265:13029–13035. [PubMed: 1695900]
22. Ehrlich HJ, Gebbink RK, Preissner KT, Keijer J, Esmon NL, Mertens K, Pannekoek H. Thrombin neutralizes plasminogen activator inhibitor 1 (PAI-1) that is complexed with vitronectin in the endothelial cell matrix. J Cell Biol. 1991; 115:1773–1781. [PubMed: 1721912]
23. Keijer J, Ehrlich HJ, Linders M, Preissner KT, Pannekoek H. Vitronectin governs the interaction between plasminogen activator inhibitor 1 and tissue-type plasminogen activator. J Biol Chem. 1991; 266:10700–10707. [PubMed: 1709939]
24. van Meijer M, Stoop A, Smilde A, Preissner KT, van Zonneveld AJ, Pannekoek H. The composition of complexes between plasminogen activator inhibitor 1, vitronectin and either thrombin or tissue-type plasminogen activator. Thromb Haemost. 1997; 77:516–521. [PubMed: 9066004]

25. Rezaie AR. Vitronectin functions as a cofactor for rapid inhibition of activated protein C by plasminogen activator inhibitor-1. Implications for the mechanism of profibrinolytic action of activated protein C. J Biol Chem. 2001; 276:15567–15570. [PubMed: 11264280]
26. Komissarov AA, Andreasen PA, Bodker JS, Declerck PJ, Anagli JY, Shore JD. Additivity in effects of vitronectin and monoclonal antibodies against alpha-helix F of plasminogen activator inhibitor-1 on its reactions with target proteinases. J Biol Chem. 2005; 280:1482–1489. [PubMed: 15516335]
27. Komissarov AA, Zhou A, Declerck PJ. Modulation of serpin reaction through stabilization of transient intermediate by ligands bound to alpha-helix F. J Biol Chem. 2007; 282:26306–26315. [PubMed: 17613529]
28. Komissarov AA, Andreasen PA, Declerck PJ, Kamikubo Y, Zhou A, Gruber A. Redirection of the reaction between activated protein C and a serpin to the substrate pathway. Thromb Res. 2008; 122:397–404. [PubMed: 18045665]
29. Sen P, Komissarov AA, Florova G, Idell S, Pendurthi UR, Vijaya Mohan RL. Plasminogen activator inhibitor-1 inhibits factor VIIa bound to tissue factor. J Thromb Haemost. 2011; 9:531–539. [PubMed: 21143380]
30. Bartha K, Declerck PJ, Moreau H, Nelles L, Collen D. Synthesis and secretion of plasminogen activator inhibitor 1 by human endothelial cells in vitro. Effect of active site mutagenized tissue-type plasminogen activator. J Biol Chem. 1991; 266:792–797. [PubMed: 1898737]
31. Bartha K, Declerck PJ, Moreau H, Nelles L, Collen D. Synthesis and secretion of plasminogen activator inhibitor 1 by human endothelial cells in vitro. Effect of active site mutagenized tissue-type plasminogen activator. J Biol Chem. 1991; 266:792–797. [PubMed: 1898737]
32. Olson ST, Swanson R, Day D, Verhamme I, Kvassman J, Shore JD. Resolution of Michaelis complex, acylation, and conformational change steps in the reactions of the serpin, plasminogen activator inhibitor- 1, with tissue plasminogen activator and trypsin. Biochemistry. 2001; 40:11742–11756. [PubMed: 11570875]
33. Lin Z, Jiang L, Yuan C, Jensen JK, Zhang X, Luo Z, Furie BC, Furie B, Andreasen PA, Huang M. Structural basis for recognition of urokinase-type plasminogen activator by plasminogen activator inhibitor-1. J Biol Chem. 2011; 286:7027–7032. [PubMed: 21199867]
34. Zhou A, Huntington JA, Pannu NS, Carrell RW, Read RJ. How vitronectin binds PAI-1 to modulate fibrinolysis and cell migration. Nat Struct Biol. 2003; 10:541–544. [PubMed: 12808446]
35. Bijnens AP, Gils A, Stassen JM, Komissarov AA, Knockaert I, Brouwers E, Shore JD, Declerck PJ. The distal hinge of the reactive site loop and its proximity: a target to modulate plasminogen activator inhibitor-1 activity. J Biol Chem. 2001; 276:44912–44918. [PubMed: 11559698]
36. Ibarra CA, Blouse GE, Christian TD, Shore JD. The contribution of the exosite residues of plasminogen activator inhibitor-1 to proteinase inhibition. J Biol Chem. 2004; 279:3643–3650. [PubMed: 14594804]
37. Idell S, Mazar A, Cines D, Kuo A, Parry G, Gawlak S, Juarez J, Koenig K, Azghani A, Hadden W, McLarty J, Miller E. Single-chain urokinase alone or complexed to its receptor in tetracycline-induced pleuritis in rabbits. Am J Respir Crit Care Med. 2002; 166:920–926. [PubMed: 12359647]
38. Komissarov AA, Mazar AP, Koenig K, Kurdowska AK, Idell S. Regulation of intrapleural fibrinolysis by urokinase-alpha-macroglobulin complexes in tetracycline-induced pleural injury in rabbits. Am J Physiol Lung Cell Mol Physiol. 2009; 297:L568–L577. [PubMed: 19666776]
39. Kvassman JO, Shore JD. Purification of human plasminogen activator inhibitor (PAI-1) from Escherichia coli and separation of its active and latent forms by hydrophobic interaction chromatography. Fibrinolysis. 1995; 9:215–221.
40. Komissarov AA, Mazar AP, Koenig K, Kurdowska AK, Idell S. Regulation of intrapleural fibrinolysis by urokinase-alpha-macroglobulin complexes in tetracycline-induced pleural injury in rabbits. Am J Physiol Lung Cell Mol Physiol. 2009; 297:L568–L577. [PubMed: 19666776]
41. Komissarov AA, Florova G, Idell S. Effects of extracellular DNA on plasminogen activation and fibrinolysis. J Biol Chem. 2011; 286:41949–41962. [PubMed: 21976662]
42. Komissarov AA, Stankowska D, Krupa A, Fudala R, Florova G, Florence J, Fol M, Allen TC, Idell S, Matthay MA, Kurdowska AK. Novel aspects of urokinase function in the injured lung: role of

alpha2-macroglobulin. Am J Physiol Lung Cell Mol Physiol. 2012; 303:L1037–L1045. [PubMed: 23064953]

43. Komissarov AA, Declerck PJ, Shore JD. Mechanisms of conversion of plasminogen activator inhibitor 1 from a suicide inhibitor to a substrate by monoclonal antibodies. J Biol Chem. 2002; 277:43858–43865. [PubMed: 12223472]
44. Olson ST, Swanson R, Day D, Verhamme I, Kvassman J, Shore JD. Resolution of Michaelis complex, acylation, and conformational change steps in the reactions of the serpin, plasminogen activator inhibitor- 1, with tissue plasminogen activator and trypsin. Biochemistry. 2001; 40:11742–11756. [PubMed: 11570875]
45. Komissarov AA, Declerck PJ, Shore JD. Protonation state of a single histidine residue contributes significantly to the kinetics of the reaction of plasminogen activator inhibitor-1 with tissue-type plasminogen activator. J Biol Chem. 2004; 279:23007–23013. [PubMed: 15033993]
46. Verhamme I, Kvassman JO, Day D, Debrock S, Vleugels N, Declerck PJ, Shore JD. Accelerated conversion of human plasminogen activator inhibitor-1 to its latent form by antibody binding. J Biol Chem. 1999; 274:17511–17517. [PubMed: 10364183]
47. Van De Craen B, Scroyen I, Vranckx C, Compernolle G, Lijnen HR, Declerck PJ, Gils A. Maximal PAI-1 inhibition in vivo requires neutralizing antibodies that recognize and inhibit glycosylated PAI-1. Thromb Res. 2012; 129:e126–e133. [PubMed: 22178065]
48. Jensen JK, Durand MK, Skeldal S, Dupont DM, Bodker JS, Wind T, Andreasen PA. Construction of a plasminogen activator inhibitor-1 variant without meapsurable affinity to vitronectin but otherwise normal. FEBS Lett. 2004; 556:175–179. [PubMed: 14706846]
49. Shore JD, Day DE, Francis-Chmura AM, Verhamme I, Kvassman J, Lawrence DA, Ginsburg D. A fluorescent probe study of plasminogen activator inhibitor-1. Evidence for reactive center loop insertion and its role in the inhibitory mechanism. J Biol Chem. 1995; 270:5395–5398. [PubMed: 7890653]
50. Kvassman JO, Verhamme I, Shore JD. Inhibitory mechanism of serpins: loop insertion forces acylation of plasminogen activator by plasminogen activator inhibitor-1. Biochemistry. 1998; 37:15491–15502. [PubMed: 9799512]
51. Kvassman JO, Verhamme I, Shore JD. Inhibitory mechanism of serpins: loop insertion forces acylation of plasminogen activator by plasminogen activator inhibitor-1. Biochemistry. 1998; 37:15491–15502. [PubMed: 9799512]
52. Lawrence DA, Olson ST, Muhammad S, Day DE, Kvassman JO, Ginsburg D, Shore JD. Partitioning of serpin-proteinase reactions between stable inhibition and substrate cleavage is regulated by the rate of serpin reactive center loop insertion into beta-sheet A [In Process Citation]. J Biol Chem. 2000; 275:5839–5844. [PubMed: 10681574]
53. Schechter I, Berger A. On the size of the active site in proteases. I. Papain. Biochem Biophys Res Commun. 1967; 27:157–162. [PubMed: 6035483]
54. Madison EL, Goldsmith EJ, Gerard RD, Gething MJ, Sambrook JF, Bassel-Duby RS. Amino acid residues that affect interaction of tissue-type plasminogen activator with plasminogen activator inhibitor 1. Proc Natl Acad Sci U S A. 1990; 87:3530–3533. [PubMed: 2110366]
55. Coombs GS, Bergstrom RC, Madison EL, Corey DR. Directing sequence-specific proteolysis to new targets. The influence of loop size and target sequence on selective proteolysis by tissue- type plasminogen activator and urokinase-type plasminogen activator. J Biol Chem. 1998; 273:4323–4328. [PubMed: 9468480]
56. Declerck PJ, Gils A. Three Decades of Research on Plasminogen Activator Inhibitor-1: A Multifaceted Serpin. Semin Thromb Hemost. 2013
57. Komissarov AA, Zhou A, Declerck PJ. Modulation of serpin reaction through stabilization of transient intermediate by ligands bound to alpha-helix F. J Biol Chem. 2007; 282:26306–26315. [PubMed: 17613529]
58. Declerck PJ, Alessi MC, Verstreken M, Kruithof EK, Juhan-Vague I, Collen D. Measurement of plasminogen activator inhibitor 1 in biologic fluids with a murine monoclonal antibody-based enzyme-linked immunosorbent assay. Blood. 1988; 71:220–225. [PubMed: 3257145]
59. Huber K. Plasminogen activator inhibitor type-1 (part one): basic mechanisms, regulation, and role for thromboembolic disease. J Thromb Thrombolysis. 2001; 11:183–193. [PubMed: 11577256]

60. Zeerleder S, Schroeder V, Hack CE, Kohler HP, Wuillemin WA. TAFI and PAI-1 levels in human sepsis. Thromb Res. 2006; 118:205–212. [PubMed: 16009400]
61. Fay WP, Murphy JG, Owen WG. High concentrations of active plasminogen activator inhibitor-1 in porcine coronary artery thrombi. Arterioscler Thromb Vasc Biol. 1996; 16:1277–1284. [PubMed: 8857925]
62. Naessens D, Gils A, Compernolle G, Declerck PJ. Elucidation of the epitope of a latency-inducing antibody: identification of a new molecular target for PAI-1 inhibition. Thromb Haemost. 2003; 90:52–58. [PubMed: 12876625]
63. Van De Craen B, Declerck PJ, Gils A. The Biochemistry, Physiology and Pathological roles of PAI-1 and the requirements for PAI-1 inhibition in vivo. Thromb Res. 2012; 130:576–585. [PubMed: 22801256]
64. Andreasen PA. PAI-1 - a potential therapeutic target in cancer. Curr Drug Targets. 2007; 8:1030–1041. [PubMed: 17896954]
65. Huang WT, Vayalil PK, Miyata T, Hagood J, Liu RM. Therapeutic value of small molecule inhibitor to plasminogen activator inhibitor-1 for lung fibrosis. Am J Respir Cell Mol Biol. 2012; 46:87–95. [PubMed: 21852684]
66. Izuhara Y, Yamaoka N, Kodama H, Dan T, Takizawa S, Hirayama N, Meguro K, van Ypersele de SC, Miyata T. A novel inhibitor of plasminogen activator inhibitor-1 provides antithrombotic benefits devoid of bleeding effect in nonhuman primates. J Cereb Blood Flow Metab. 2010; 30:904–912. [PubMed: 20087372]
67. Aleman C, Alegre J, Monasterio J, Segura RM, Armadans L, Angles A, Varela E, Ruiz E, Fernandez dS. Association between inflammatory mediators and the fibrinolysis system in infectious pleural effusions. Clin Sci (Lond). 2003; 105:601–607. [PubMed: 12826021]
68. Green J, Doughty L, Kaplan SS, Sasser H, Carcillo JA. The tissue factor and plasminogen activator inhibitor type-1 response in pediatric sepsis-induced multiple organ failure. Thromb Haemost. 2002; 87:218–223. [PubMed: 11858480]
69. Raeven P, Feichtinger GA, Weixelbaumer KM, Atzenhofer S, Redl H, Van GM, Bahrami S, Osuchowski MF. Compartment-specific expression of plasminogen activator inhibitor-1 correlates with severity/outcome of murine polymicrobial sepsis. Thromb Res. 2012; 129:e238–e245. [PubMed: 22381165]
70. Raaphorst J, Johan Groeneveld AB, Bossink AW, Erik HC. Early inhibition of activated fibrinolysis predicts microbial infection, shock and mortality in febrile medical patients. Thromb Haemost. 2001; 86:543–549. [PubMed: 11522001]
71. Zeerleder S, Hack CE, Wuillemin WA. Disseminated intravascular coagulation in sepsis. Chest. 2005; 128:2864–2875. [PubMed: 16236964]
72. Madoiwa S, Nunomiya S, Ono T, Shintani Y, Ohmori T, Mimuro J, Sakata Y. Plasminogen activator inhibitor 1 promotes a poor prognosis in sepsis-induced disseminated intravascular coagulation. Int J Hematol. 2006; 84:398–405. [PubMed: 17189219]
73. Zeerleder S, Schroeder V, Hack CE, Kohler HP, Wuillemin WA. TAFI and PAI-1 levels in human sepsis. Thromb Res. 2006; 118:205–212. [PubMed: 16009400]
74. Shapiro NI, Schuetz P, Yano K, Sorasaki M, Parikh SM, Jones AE, Trzeciak S, Ngo L, Aird WC. The association of endothelial cell signaling, severity of illness, and organ dysfunction in sepsis. Crit Care. 2010; 14:R182. [PubMed: 20942957]
75. Seiffert D, Loskutoff DJ. Kinetic analysis of the interaction between type 1 plasminogen activator inhibitor and vitronectin and evidence that the bovine inhibitor binds to a thrombin–derived amino-terminal fragment of bovine vitronectin. Biochim Biophys Acta. 1991; 1078:23–30. [PubMed: 1710930]

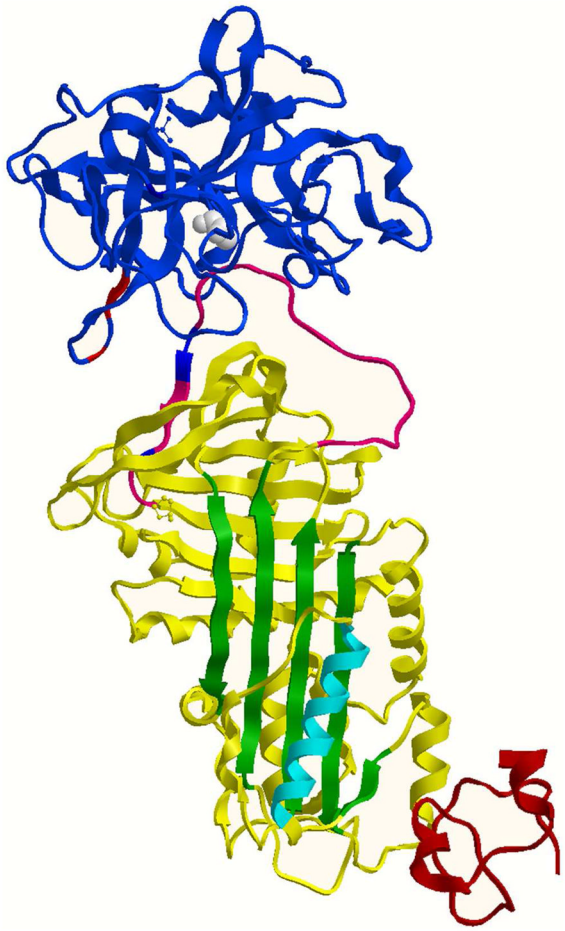

Figure 1. The proposed ribbon model of S195A tcuPA/PAI-1/Vn "Molecular Sandwich" type complex

Crystal structures of PAI-1 (yellow) complexes with S195A tcuPA (blue) (33), and SMB domain of Vn (brown) (34) were used. The exposed RCL of active PAI-1 is shown in red with positions of E350 and E351 (P4′P5′ nomenclature of Schechter and Berger (53)) in blue, β-sheet A in green and a-helix F in cyan. Active site A195 of S195A tcuPA is shown as a white space-filled residue, and positions of positively charged residues of 37-loop of uPA are red.

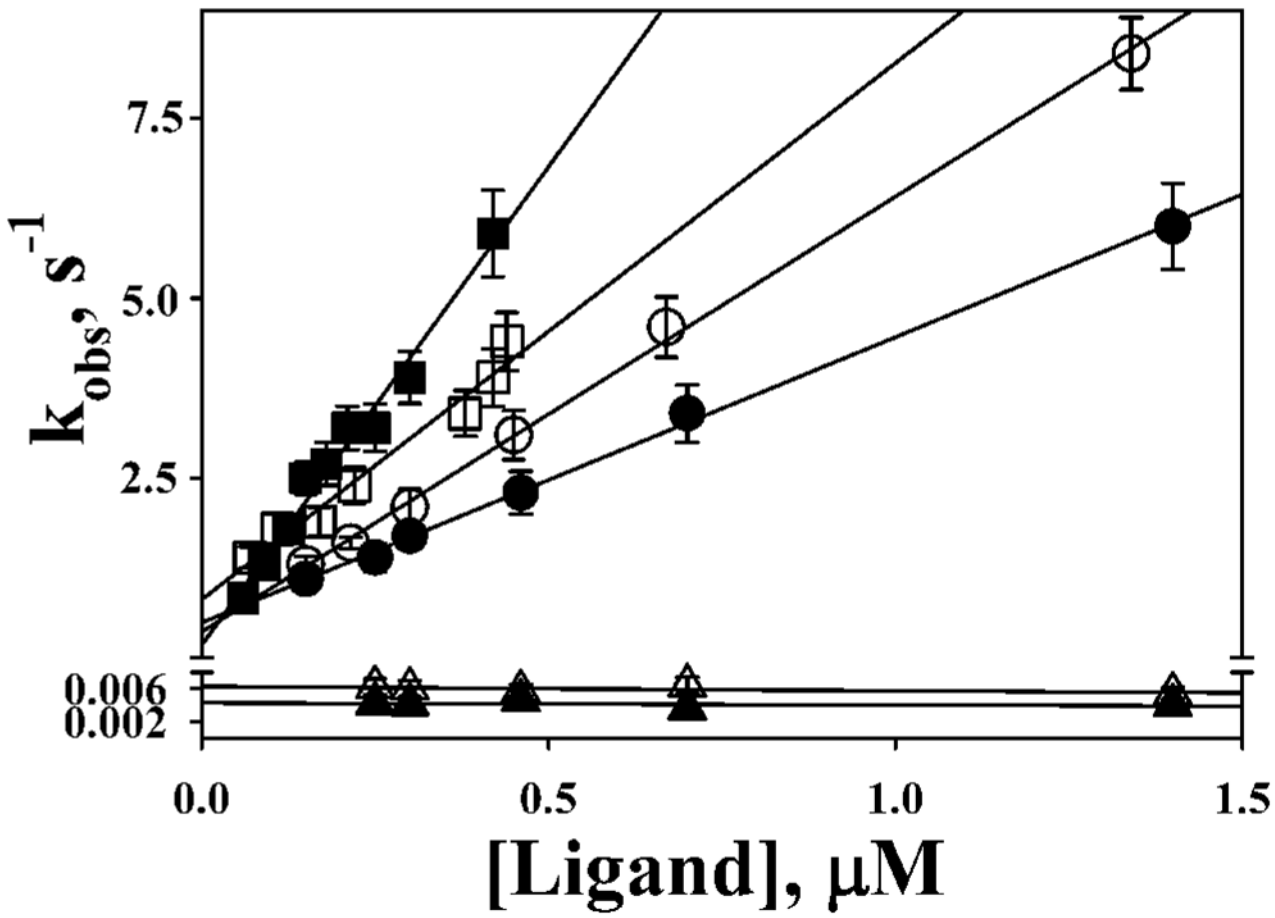

Figure 2. Rapid association of PAI-1 and ligands and slow dissociation of S195A tcuPA

Linear dependences of k_{obs} from [ligand] for the association of PAI-1 and its complexes with ligands (k_{+n}; n=1–4; Scheme 1). Values of k_{+n} for the interaction of S195A tcuPA with NBD P1′ PAI-1 (○); Vn and NBD S119C PAI-1 (□); S195A tcuPA with NBD P1′ PAI-1/Vn (●), and Vn with NBD S119C PAI-1/S195A tcuPA (■) were calculated from the slopes of the best linear fit to the data (Table 1). Slow dissociation of S195A tcuPA limits the reaction between tPA and complex of NBD P9 PAI-1 with S195A tcuPA (△) and MSC (complex of NBD P9 PAI-1 with S195A tcuPA and Vn; Scheme 1) (▲).

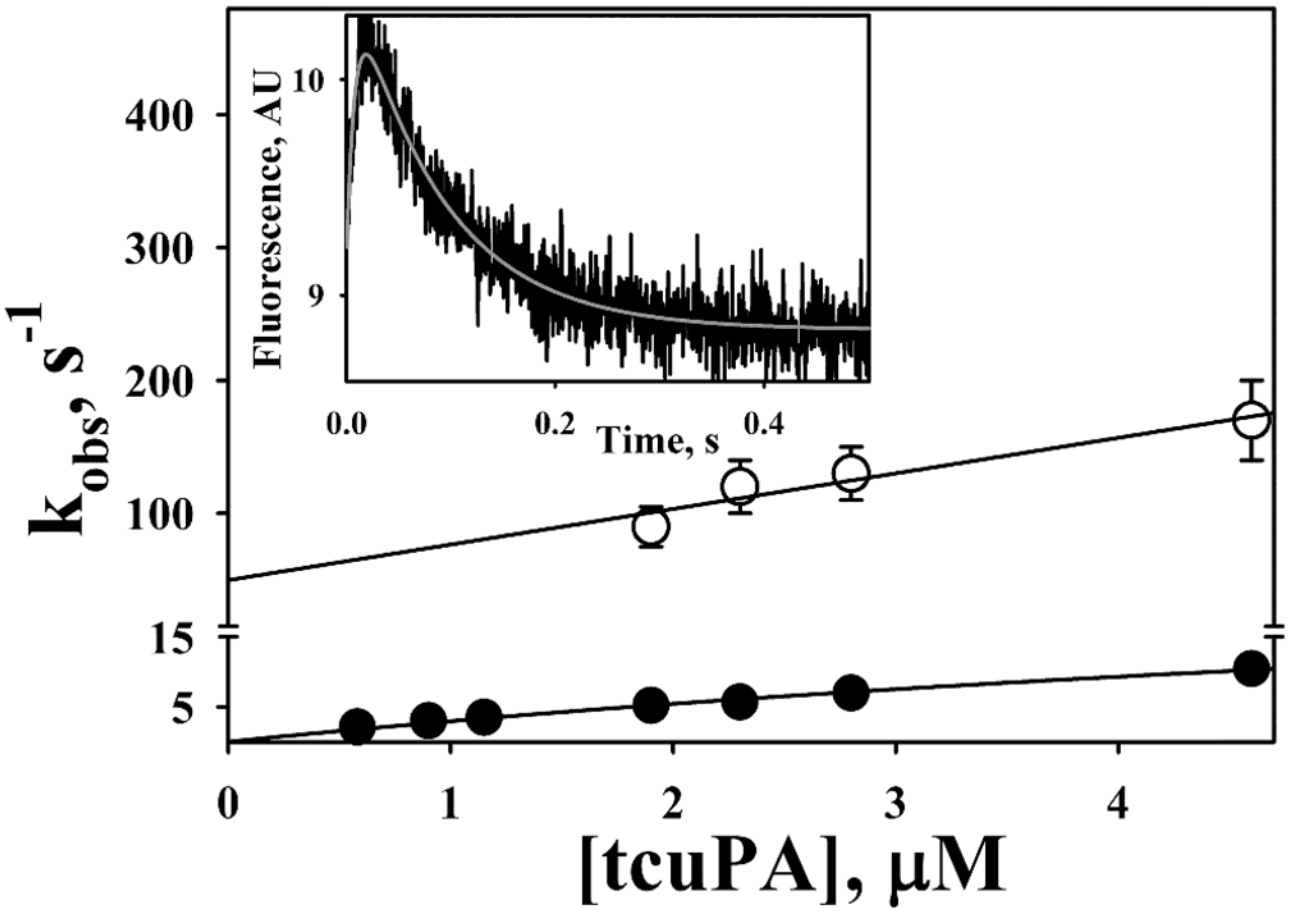

Figure 3. NBD-labeled cysteine at position P1′ of RCL of PAI-1 affects the kinetics of inhibition of tcuPA

The dependences of k_{obs} for the fast step (an increase in NBD fluorescence emission) (○), and slow step (a decrease in the NBD fluorescence emission) (●) on enzyme concentration. The solid lines represent the best fit of the linear equation $k_{obs2} = (k_{lim}+k_{-1}) + k_1[tcuPA]$ (r^2=0.93) (fast step), and a hyperbolic equation $k_{obs1} = k_{lim}*[tcuPA]/(K_m + [tcuPA])$ (r^2=0.99) (slow step) to the data by SigmaPlot 11.0. The values of k_{lim} and Km (Scheme 2) were 33.3 ± 5.2 s^{-1}, and 10.2 ± 2.2 μM, respectively. The slope and intercept of the linear dependence of k_{obs} on enzyme concentration represent a second order rate constant for the interaction of tcuPA with NBD P1′ PAI-1 k_{+1} = 26.8 ± 2.8 μM^{-1} s^{-1}, and ($k_{lim}+k_{-1}$) = 50 ± 8 s^{-1}, respectively. **Inset:** Trace of the changes in NBD fluorescence for the reaction of NBD P1′ PAI-1 (0.12 μM) with 2.0 μM tcuPA. Values of k_{obs1} and k_{obs2} were calculated by fitting (grey line) a double exponential equation to the time traces of changes in NBD-fluorescence emission using SigmaPlot 11.0.

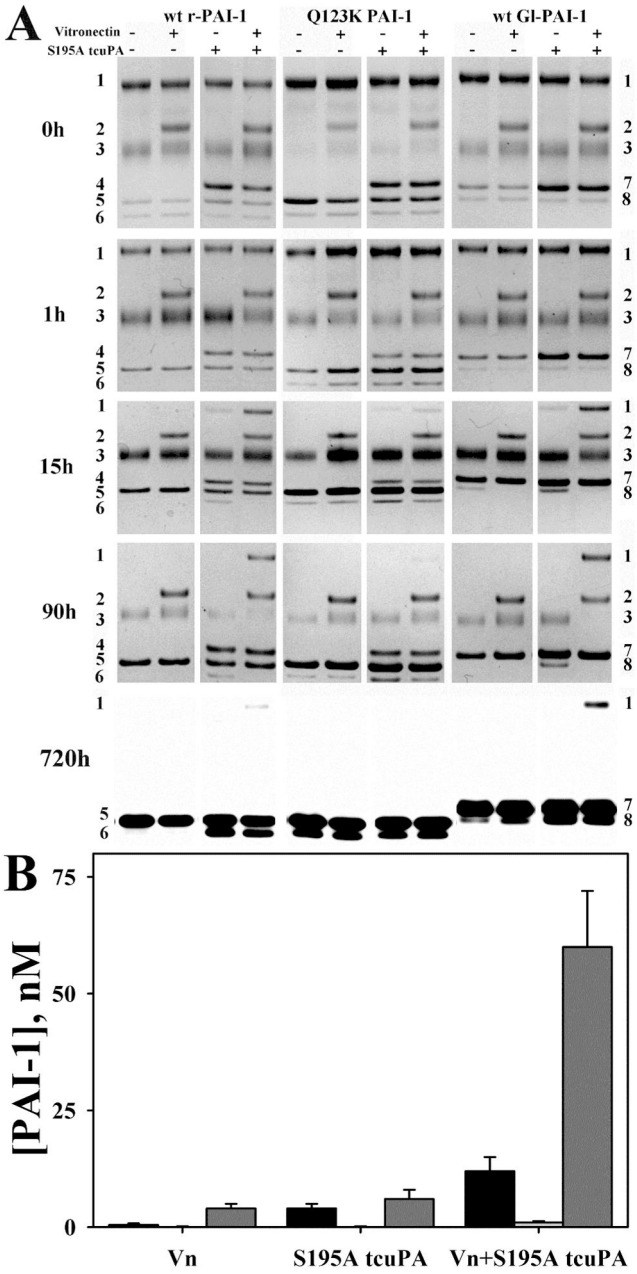

Figure 4. Tremendous stabilization of active PAI-1 in MSC under physiological conditions

(**A**) SDS PAGE analysis of products of the reaction between sctPA and rPAI-1, Q123K PAI-1, and Gl-PAI-1 and their complexes with Vn, S195A tcuPA, and both ligands (the table at the top of the gels.) incubated for 0, 1, 15, 90 (stained with SYRRO Ruby) and 720 h (PAI-1 antigen was visualized with Western blot analysis) at 37°C. Positions of PAI-1/tPA SIC (1), Vn (2), tPA (3), S195A tcuPA (4), latent and cleaved rPAI-1 (5 and 6, respectively), co-migrating S195A tcuPA and latent Gl-PAI-1 (7), cleaved Gl-PAI-1 (8), are indicated to the left (rPAI-1 and Q123K PAI-1) and to the right (Gl-PAI-1) of the gels. (**B**) Active PAI-1 concentration in the reaction mixtures, shown in the Western blot (**A**, lower panel) was estimated by inhibiting the activation of Plg by uPA, as described elsewhere (9;41). After incubation with both Vn and S195A tcuPA for 1 month (720h) at 37°C rPAI-1

(filled bars) and Gl-PAI-1 (gray bars), but not Q123K PAI-1 (empty bars) inhibit the activation of Plg by uPA.

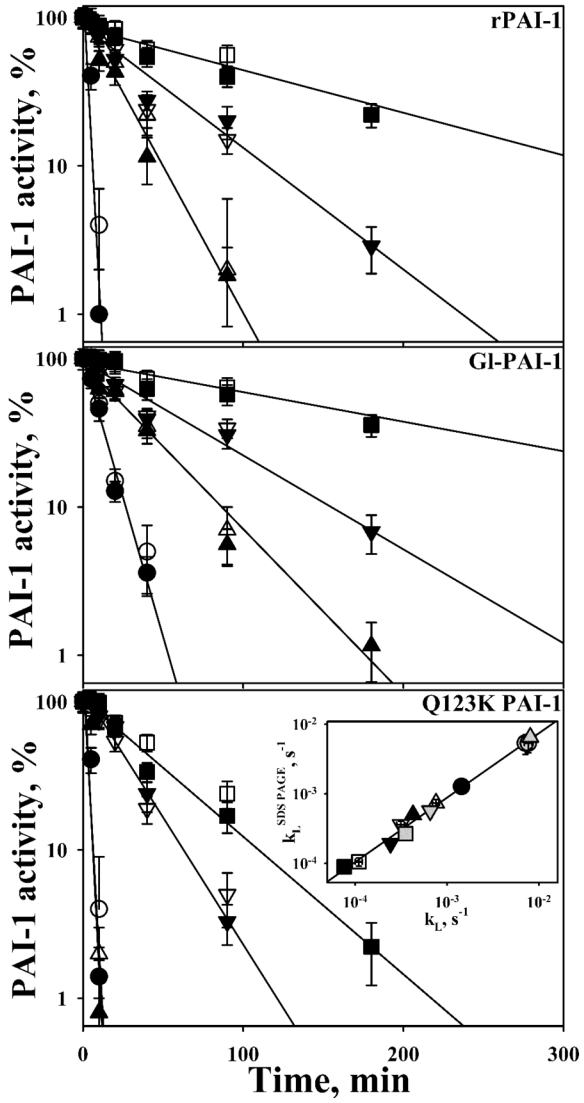

Figure 5. Spontaneous inactivation of rPAI-1, Q123K PAI-1, and Gl-PAI-1 (circles) and their complexes with Vn (triangles), S195A tcuPA (reversed triangles), and both ligands (squares) at 50°C

The concentration of active PAI-1 was determined from the residual tPA amidolytic activity after titrating the sample with increasing amounts of sctPA as described under Experimental Procedures and plotted on a semilogarithmic scale (filled symbols). Separate aliquots were incubated with an excess of sctPA and the products of the reaction were separated by SDS PAGE, as shown in Figure 4 and described under Experimental Procedures. The amounts of active PAI-1 were estimated from relative density of SIC, latent and cleaved PAI-1 on gels and plotted as empty symbols. Linear equations were fit to both sets of data (solid lines represent the best fits to filled symbols) using SigmaPlot 11.0, and the first order rate constants (k_{L1}, k_{L2}, k_{L3}, k_{L4} (Table 2), and $k_{L1}^{SDS\ PAGE}$, $k_{L2}^{SDS\ PAGE}$, $k_{L3}^{SDS\ PAGE}$, $k_{L4}^{SDS\ PAGE}$ respectively, Scheme 1) were calculated from the slopes. **Inset:** Correlation between values of k_L measured by two different methods. The values of k_L estimated from the results of SDS PAGE analysis were plotted against the corresponding values obtained from titrating the reaction mixtures with sctPA: rPAI-1 (empty symbols), Gl-PAI-1 (black symbols), and Q123K PAI-1 (grey symbols). Data for free rPAI-1, Gl-PAI-1, and Q123K

PAI-1 are shown as circles, for their complexes with Vn as triangles, with S195A tcuPA as reversed triangles, and for both ligands as squares. The solid line represents the best linear fit to the data of linear equation ($k_L^{\text{SDS PAGE}} = -0.27 + 0.93\ k_L$; $r^2 = 0.99$).

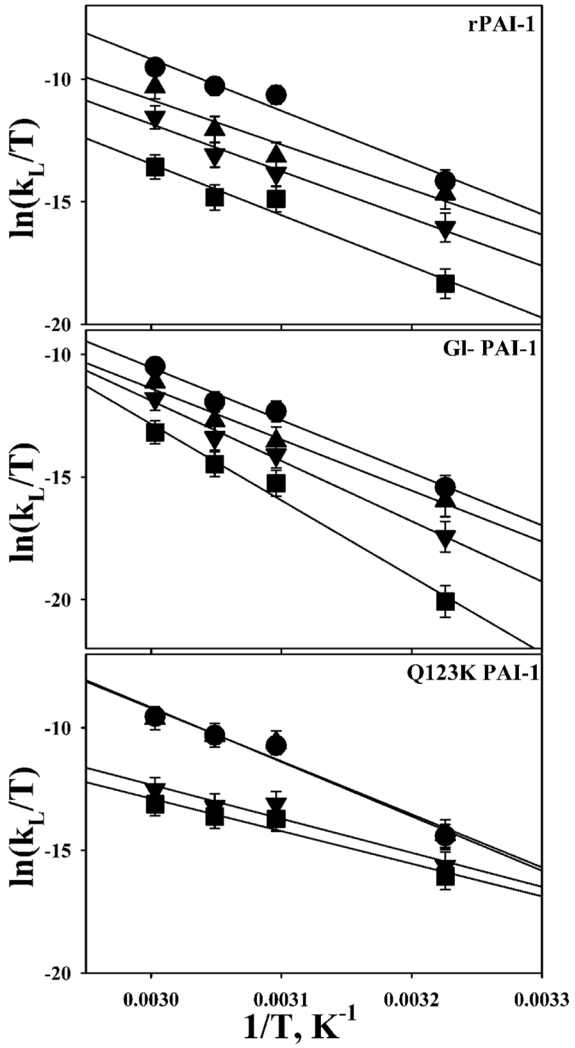

Figure 6. Eyring Plots for the spontaneous inactivation of PAI-1 alone (circles), and in the presence of Vn (triangles), S195A tcuPA (reversed triangles) and both ligands (squares)

Corresponding k_L have been determined at 37, 50, 55 and 60°C as described under Experimental Procedures (Table 2). Solid lines represent the best fit of the linear equation to the data. Values of the activation enthalpy ($\Delta H^{\ddagger}$) and entropy ($\Delta S^{\ddagger}$) (Table 3) were determined as -(slope)xR and (intercept - ln(k_B/h))xR, where R, k_B, and h are 8.3145 J/mol, 1.3806×10^{-23} J/K and 6.626×10^{-34} J/s, respectively.

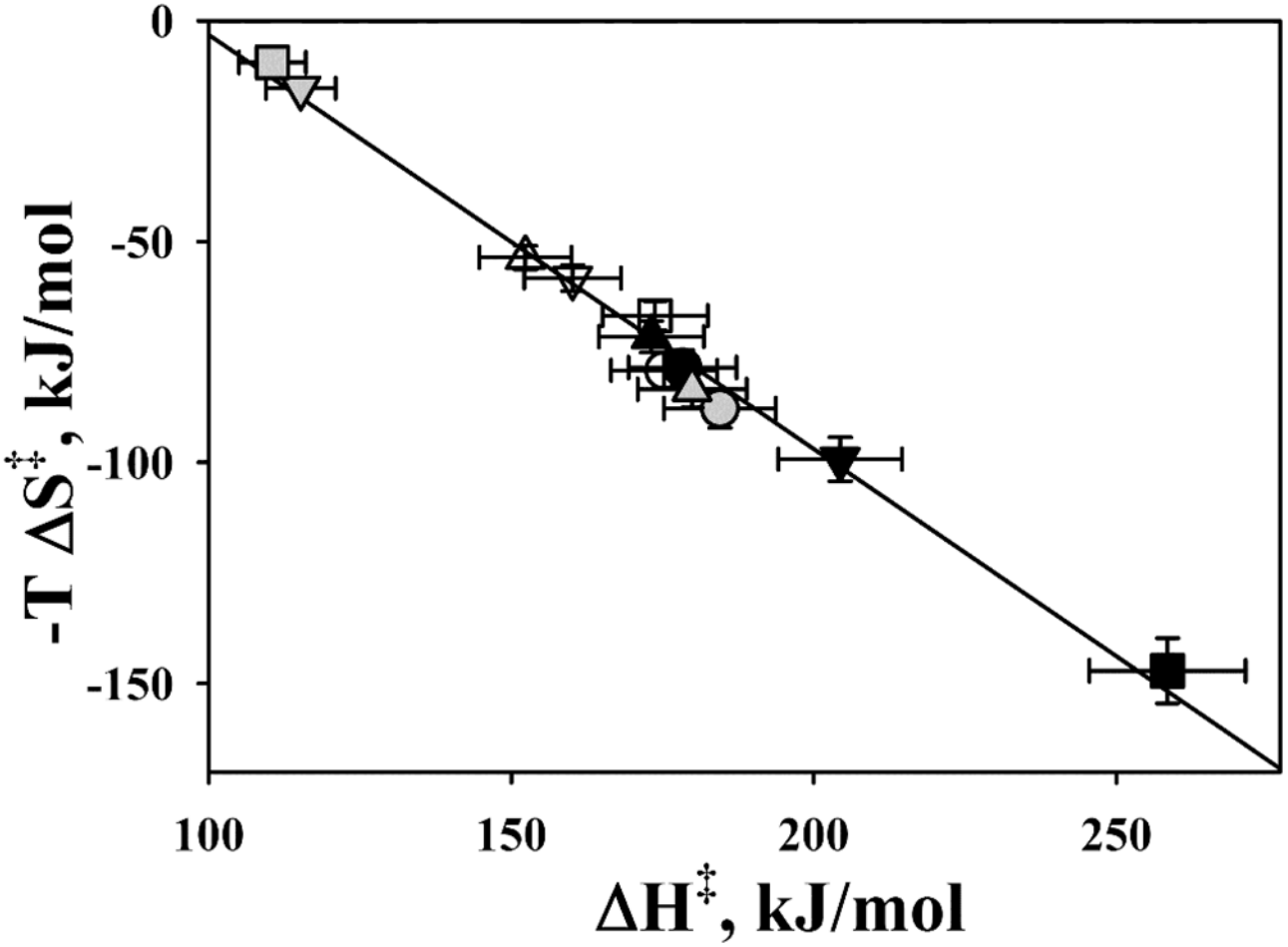

Figure 7. Enthalpy-entropy compensation

A linear correlation between changes in the contribution of $-T\Delta S^{\ddagger}$ and $\Delta H^{\ddagger}$ (Table 3) to $\Delta G^{\ddagger}$ for the three PAI-1 variants and their complexes with ligands at 37°C. The values of $-T\Delta S^{\ddagger}$ for rPAI-1 (empty symbols), Gl-PAI-1 (black symbols), and Q123K PAI-1 (grey symbols) for free serpins (circles), and their complexes with Vn (triangles), S195A tcuPA (reversed triangles), and both ligands (squares) were plotted as a function of $\Delta H^{\ddagger}$. The solid line represents the best fit of the linear equation ($-T\Delta S^{\ddagger} = 90.6 - 0.94\ \Delta H^{\ddagger}$; $r^2 = 0.99$) to the data.

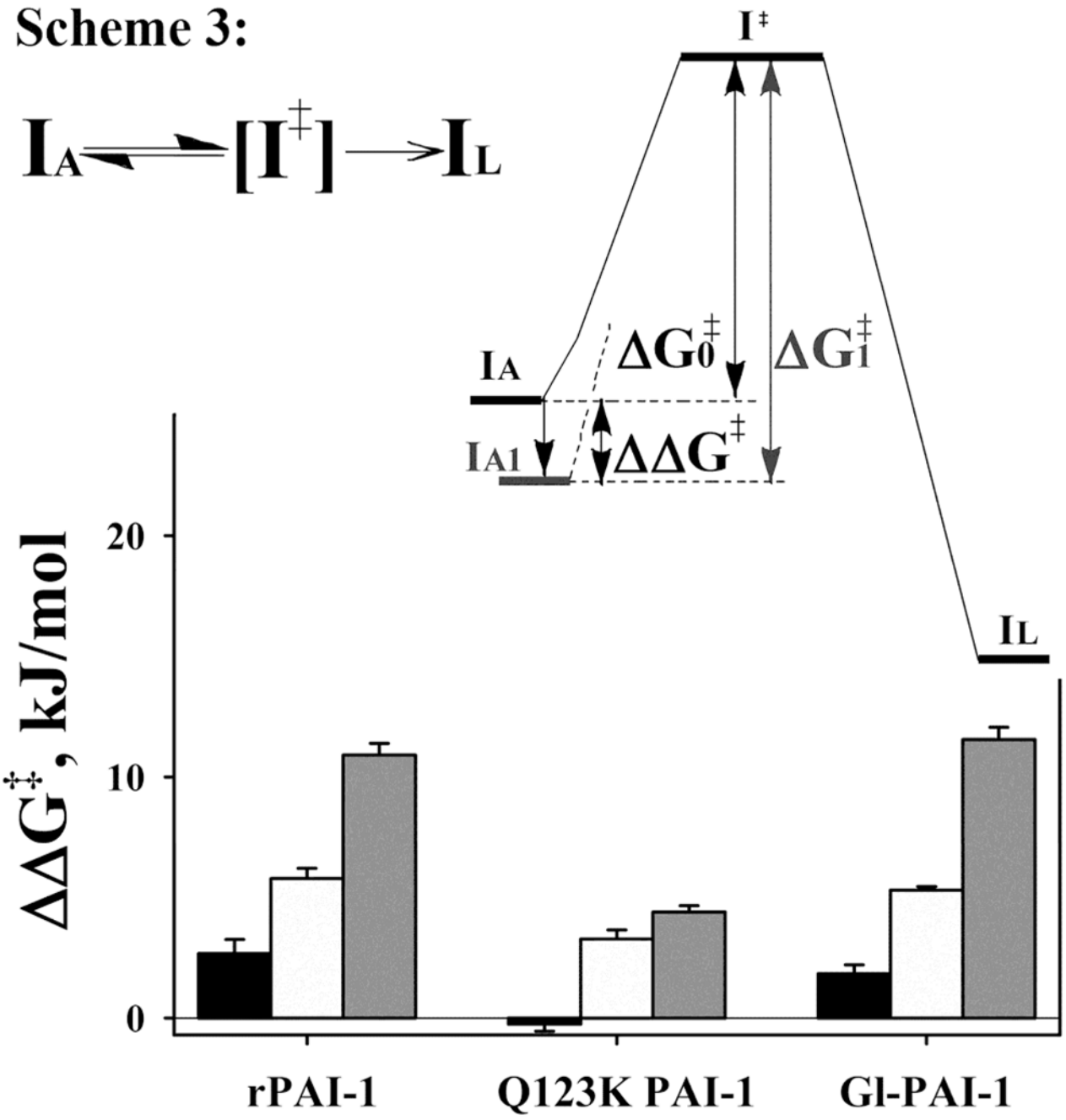

Figure 8. Synergistic stabilization of the active conformation of PAI-1 in MSC

Scheme 3: A transition intermediate ($I^{\ddagger}$), which is in equilibrium with the active PAI-1 (I_A), forms during conformational changes accompanying the transition to the latent conformation (I_L) (46). A diagram depicts how I_A is stabilized in the complex with ligand(s) (I_{A1}) due to an increase in the $\Delta G^{\ddagger}$ ($\Delta\Delta G^{\ddagger} = \Delta G^{\ddagger}_1 - \Delta G^{\ddagger}_0$), where $\Delta G^{\ddagger}_1$ and $\Delta G^{\ddagger}_0$ are changes in the activation Gibbs free energy for active PAI-1 with and without ligand(s), respectively. A bar graph shows the contribution of Vn (black), S195A tcuPA (white), and both ligands (gray) to $\Delta\Delta G^{\ddagger}$ for rPAI-1, Q123K PAI-1, and Gl-PAI-1 at 37°C. The values of $\Delta G^{\ddagger}_0$ and $\Delta G^{\ddagger}_1$ were calculated as $\Delta G^{\ddagger} = \Delta H^{\ddagger} - T\Delta S^{\ddagger}$ (Table 3).

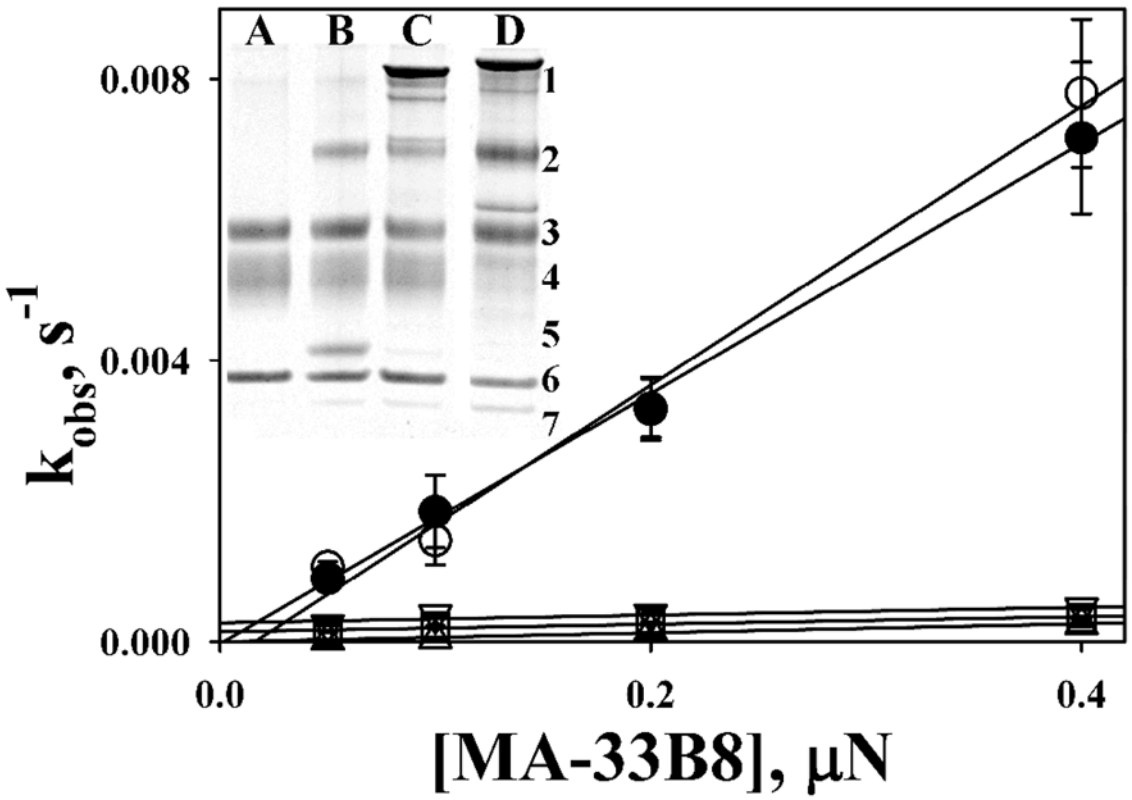

Figure 9.

MSCs formed with S195A tcuPA and mAbs protect rPAI-1/Vn from inactivation by MA-33B8 and spontaneous active to latent transition. Dependences of k_{obs} for RCL insertion for NBD P9 PAI-1 (○), NBD P9 PAI-1/Vn (●) and MSCs with MA-56A7C10 (△), MA-44E4 (□), and S195A tcuPA (▽) on [MA-33B8]. NBD P9 PAI-1, its complex with Vn (10 nM), and MSCs formed in presence of 20 nM of S195A tcuPA or a mAb (MA-56A7C10 or MA-44E4) were incubated with MA-33B8 (50–400 nN) in 96-well flat bottom plates from Costar (Corning Inc) and an increase in NBD fluorescence with time was registered using a fluorescence spectrophotometer SynergyTM HT Hybrid Reader. The k_{obs} were calculated by fitting a single exponential equation to the data using Gen5™ 2.0 Data Analysis Software (BioTek) and SigmaPlot 11.0 (SPSS Inc.), as described elsewhere (26;43;45). **Inset:** Stabilization of rPAI-1/Vn (lane A) in MSCs with S195A tcuPA (lane B), MA-56A7C10 (lane C), and MA-42A2F6 (lane D) after incubation at 37°C for 168 h (one week). Active PAI-1 was quenched by sctPA and reaction mixtures were analyzed as described under Experimental Procedures. Positions of mAb (1), PAI-1/tPA SIC (2), Vn (3), tPA (4), S195A tcuPA (5), latent (6) and cleaved PAI-1 (7) are indicated to the right of the gel.

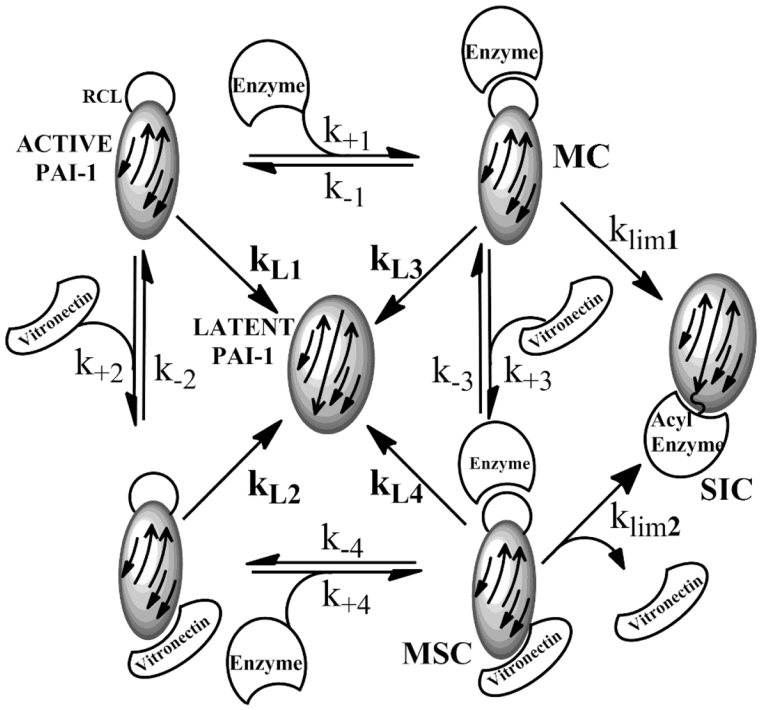

Scheme 1.

A transient ternary "Molecular Sandwich" type complex (MSC) is a part of the PAI-1 inhibitory mechanism *in vivo*.

Mechanism-based inactivation of the enzyme by PAI-1 and PAI-1/Vn results in a stable inhibitory complex (SIC). Formation of the acyl-enzyme from a Michaelis complex (MC) or MSC triggers fast insertion (k_{lim1}, or k_{lim2}, respectively) of the reactive center loop (RCL) into central β-sheet A (arrows) as strand 3A (central arrow), translocation of the enzyme to the opposite pole of the PAI-1 molecule, and stabilization of the acyl-enzyme as SIC. A decrease in k_{lim2} (k_{lim2}=0 for S195A tcuPA) results in a stable ternary MSC (k_{+n} and k_{-n} are association and dissociation rate constants, respectively). Inactive, latent PAI-1 forms due to the slow spontaneous insertion of RCL into central β-sheet A (k_{L1}, k_{L2}, k_{L3}, k_{L4} for free PAI-1, PAI-1 in the presence of Vn, S195A tcuPA, or both ligands, respectively).

Scheme 2.
Two step inactivation of proteianase (E) by PAI-1 (I)

Table 1

The values of the association and dissociation rate constants (k_{+1}, k_{+2}, k_{+3}, k_{+4} and k_{-1}, k_{-2}, k_{-3}, k_{-4} respectively); and dissociation equilibrium constants ($K_D = k_-/k_+$) for the interactions between wt PAI-1, its mutant variants, and their complexes with S195A tcuPA and Vn at 25°C.

Step (Scheme 1)	Ligand	PAI-1 variant	k_+ $\mu M^{-1}s^{-1}$	$k_- \times 10^{-3}$ s^{-1}	$K_D = k_-/k_+$ nM
k_1	S195A tcuPA	wt rPAI-1	5.4[a]	7.0 ± 0.4[b]	1.3 ± 0.4[c]
		Gl-PAI-1	4.2[a]	5.0 ± 0.3[b]	1.2 ± 0.5[c]
		Q123K PAI-1	4.6[a]	6.0 ± 0.4[b]	1.3 ± 0.5[c]
		NBD P9 PAI-1	7.3 ± 0.2[d]	6.0 ± 0.3[e]	1.2 ± 0.6[f]
		NBD P1′ PAI-1	6.1 ± 0.2[d]	150 ± 20[e]	24.6[g]
		NBD S119C PAI-1	5.0 ± 0.2[d]	ND[h]	ND[h]
		P4′P5′/AA NBD P9 PAI-1	2.8 ± 0.2 [i]	7.0 ± 0.2[e]	2.5[g]
k_2	Vn	NBD S119C PAI-1	7.2 ± 0.3[d]	2.2–7.2 [a]	0.3–1.0[j]
k_3	Vn	NBD S119C PAI-1	13.3 ± 0.3[d]	ND[h]	ND[h]
k_4	S195A tcuPA	wt-rPAI-1	4.3[a]	3.0 ± 0.2[b]	0.7 ± 0.3[c]
		Gl-PAI-1	5.0[a]	4.0 ± 0.3[b]	0.8 ± 0.4[c]
		Q123K PAI-1[k]	4.6[a]	6.0 ± 0.3[b]	1.3 ± 0.3[c]
		NBD P9 PAI-1	8.0 ± 0.3[d]	4.0 ± 0.2[e]	0.9 ± 0.4[f]
		NBD P1′ PAI-1	4.0 ± 0.2[d]	90 ± 10[e]	22.5[g]
		NBD S119C PAI-1	5.0 ± 0.2[d]	ND[h]	ND[h]
		P4′P5′/AA NBD P9 PAI-1	ND[h]	4.0 ± 0.2[e]	ND[h]

[a] estimated from K_D and k_{+1} and k_{+4} or k_{-1} and k_{-4} values;

[b] measured by the reaction of preformed unlabeled PAI-1 variant/ligand(s) complexes with an excess of NBD P1′ PAI-1;

[c] estimated from the dependence of the initial amidolytic activity of tPA after its reaction with an equimolar PAI-1 variant (its complex with Vn) incubated with increasing amounts of S195A tcuPA;

[d] determined from the slopes of linear dependences of k_{obs} versus [ligand] for the interaction of NBD labeled variants of PAI-1 (their complexes) with a corresponding ligand (Figure 2);

[e] determined from k_{obs} (independent on proteinase concentration) for the reaction of the preformed complex NBD PAI-1/ligand(s) with an excess of sctPA or tcuPA (Figure 2);

[f] determined from the dependence of k_{obs} on [S195A tcuPA] for the reaction of an excess of tctPA with NDB P9 PAI-1 preincubated with different amounts of S195A tcPAI-1 as described previously (43);

[g] calculated as k_-/k_+;

[h] not determined;

[i] k_{+1} for association of P4′P5′/AA PAI-1 with tcuPA (36);

[j] K_D for binding Vn to wt PAI-1 (34;75);

[k] Q123K PAI-1 possesses low affinity towards Vn (48).

Table 2

Values of k_{L1}, k_{L2}, k_{L3} and k_{L4} (Scheme 1) for rPAI-1, Q123K PAI-1, Gl-PAI-1 and their complexes with Vn, S195A tcuPA and both ligands, determined at different temperatures.

		k_L, $\times 10^{-3}$ s^{-1}			
Ligand PAI-1	**t °C**	**none (k_{L1})**	**Vn (k_{L2})**	**S195A tcuPA (k_{L3})**	**Vn+S195A tcuPA (k_{L4})**
rPAI-1	37	0.22 ± 0.03	0.13 ± 0.02	0.033 ± 0.004	0.0034 ± 0.0005
	50	7.7 ± 0.6	0.76 ± 0.06	0.32 ± 0.04	0.11 ± 0.02
	55	11.2 ± 1.5	1.9 ± 0.2	0.68 ± 0.08	0.12 ± 0.01
	60	24.6 ± 1.8	11.0 ± 1.5	3.2 ± 0.3	0.42 ± 0.03
Q123K PAI-1	37	0.17 ± 0.02	0.18 ± 0.02	0.050 ± 0.006	0.033 ± 0.005
	50	7.1 ± 1.4	8.1 ± 1.4	0.66 ± 0.07	0.36 ± 0.04
	55	11.0 ± 1.0	10.9 ± 1.0	0.60 ± 0.03	0.40 ± 0.03
	60	24.0 ± 2.3	22.2 ± 2.3	1.22 ± 0.10	0.67 ± 0.07
Gl-PAI-1	37	0.062 ± 0.005	0.036 ± 0.003	0.008 ± 0.001	0.0006 ± 0.0001
	50	1.44 ± 0.10	0.43 ± 0.03	0.24 ± 0.03	0.077 ± 0.008
	55	2.16 ± 0.18	1.0 ± 0.11	0.50 ± 0.03	0.17 ± 0.02
	60	9.3 ± 1.1	4.9 ± 0.5	2.5 ± 0.3	0.63 ± 0.07

[a] values of k_{L1}, k_{L2}, k_{L3} and k_{L4} were determined from semilogarithmic plots of residual PAI-1 activity versus time (Figure 5) as described under Experimental Procedures.

Table 3

The values of activation enthalpy ($\Delta H^{\ddagger}$), entropy ($\Delta S^{\ddagger}$) and the Gibbs free activation energy ($\Delta G^{\ddagger}$) for the reaction of spontaneous active to latent transition for wt rPAI-1, Q123K PAI-1, and wt Gl-PAI-1 and their complexes with Vn, S195A tcuPA and both ligands at 37°C

	Ligand(s)		$\Delta H^{\ddagger}$ [a]	$\Delta S^{\ddagger}$ [b]	$\Delta G^{\ddagger}$ [c]
Serpin	**S195A tcuPA**	**Vn**	**kJ/mol**	**J/mol K**	**kJ/mol**
rPAI-1	−	−	175.3 ± 12.8	255.5 ± 16.7	96.1
Q123K PAI-1	−	−	184.5 ± 14.2	283.2 ± 19.7	96.7
Gl-PAI-1	−	−	178.3 ± 11.4	253.3 ± 18.3	99.8
rPAI-1	−	+	152.4 ± 9.6	173.0 ± 14.0	98.7
Q123K PAI-1	−	+	179.9 ± 11.0	269.1 ± 17.3	96.4
Gl-PAI-1	−	+	173.1 ± 12.7	230.8 ± 15.7	101.6
rPAI-1	+	−	160.1 ± 9.8	188 ± 13.3	101.8
Q123K PAI-1	+	−	115.2 ± 8.4	49.2 ± 4.7	100.0
Gl-PAI-1	+	−	204.3 ± 16.6	320.2 ± 24.7	105.1
rPAI-1	+	+	173.8 ± 10.6	215.4 ± 16.7	107.0
Q123K PAI-1	+	+	110.5 ± 9.4	30.5 ± 2.7	101.1
Gl-PAI-1	+	+	258.5 ± 16.7	474.6 ± 25.6	111.3

[a] values of activation enthalpy $\Delta H^{\ddagger}$ were calculated from linear (r^2>0.9) Eyring plots (Figure 6) as - (slope)×8.3145 J/mol;

[b] values of activation entropy $\Delta S^{\ddagger}$ were calculated from Eyring plots (Figure 6) as (intercept - 23.76)×8.3145 J/mol K;

[c] values of $\Delta G^{\ddagger}$ at 37°C were calculated as $\Delta G^{\ddagger} = \Delta H^{\ddagger} - T\Delta S^{\ddagger}$